Algebraic K-Space Identification 2D technique for the automatic extraction of complex k-space of 2D structures in presence of uncertainty

Thomas Brion, Xuefeng Li, Pascal Fossat, Mohamed Ichchou, Olivier Bareille, Abdel-Malek Zine

Algebraic K-Space Identification 2D technique for the automatic extraction of complex k-space of 2D structures in presence of uncertainty

Thomas Brion[a,*], Xuefeng Li[a,c,*], Pascal Fossat[a], Mohamed Ichchou[a], Olivier Bareille[a], Abdel-Malek Zine[b]

[a] *LTDS, UMR-CNRS 5513, École Centrale de Lyon, Écully, France*
[b] *Institut Camille Jordan, UMR-CNRS 5208, École Centrale de Lyon, Écully, France*
[c] *The Marcus Wallenberg Laboratory for Sound and Vibration Research (MWL), Department of Engineering Mechanics, KTH Royal Institute of Technology, Stockholm, Sweden*

Abstract

A robust inverse method for the complex wavenumber space (complex k-space) extraction is essential for structural vibration and damping analysis of two-dimensional structures. Most existing methods suffer from extracting the reliable complex k-space of plates in the presence of realistic uncertainties, especially for plates with low damping properties. To this end, this paper presents a new method for extracting the dispersion and damping characteristics of two-dimensional periodic structures using only the full-field displacement fields as input. The proposed method, the Algebraic K-Space Identification 2D technique (AKSI 2D), is an extension of the Algebraic Wavenumber Identification technique to solve two-dimensional problems. The optimised formulas are developed within the algebraic identification framework, which allows the extraction of all the properties of the complex k-space in a comprehensive way. The proposed method is validated numerically and experimentally, and its performances are compared with other popular k-space identification methods under different uncertainty conditions. The test cases cover analytically solved isotropic fields to numerically solve orthotropic fields and finally experimental measurements. The different cases show promising results and demonstrate that the proposed method is a robust tool to characterise the wave propagation of two-dimensional structures under stochastic structural and constitution conditions.

Keywords: Inverse method, Complex k-space, Wave propagation, Uncertainty, Periodic plates

1. Introduction

With the rapid development of metastructures and composite structures, there is a growing demand for a reliable approach to characterise the wave propagation properties of these complex structures. Their complexity is often increased by the inherent presence of uncertainties. The accurate estimation of wave propagation will provide significant insight for damage detection [1] or material identification [2].

Metastructures, and in particular periodic metastructures, consist of spatially periodic patterns of assemblies of homogeneous or heterogeneous materials. The contrast between the materials and the geometric periodicity enable such materials to exhibit unusual properties. Indeed, homogeneous or uniform domains do not present band gaps specific behaviour for wave attenuation [3]. Hence, since these materials and assemblies are developed for their wave-propagation and dynamic structural abilities, the complex wavenumber is an important representative parameter. For two-dimensional structures, especially the anisotropic ones, wave propagation is direction dependent. The corresponding set of wavenumbers is called k-space. The real part of the k-space describes the spatial phase variation, whereas the imaginary part of the k-space is more related to the energy propagation (e.g. damping and transmission loss factor). The Floquet and Bloch theorems [4, 5, 6] provide a definition of wavenumbers and k-space for periodic metastructures.

*Corresponding author.
Email address: thomas.brion@ec-lyon.fr (Thomas Brion), xuefengl@kth.se (Xuefeng Li)

In the literature, there are already a lot of inverse methods to extract k-space from structural responses in different dimensions. The first class of nonlinear methods is the Fourier-based approach. In particular, the most classical one is the Fourier transform [7, 8, 9], as the wavenumber is the equivalent of angular frequency for space. It is an integral transform that maps a time or space function into its reciprocal domain. The Fast Fourier Transform (FFT) is an algorithm that allows an efficient computation of the Fourier transform. However, it is not adapted to extract the imaginary part of k-space, which is an important parameter to reflect the energy propagation in the structures. In addition, the Fourier transform would be ideal for infinite domains. But in practice, the domains are bounded, and therefore leakage effects occur. A solution to reduce this effect is to replace the rectangular windowing function with another, such as a Hanning or a Hamming windowing function [10, 11]. Based on the Fourier transform, some methods have been developed to improve its k-space computation.

A notable Fourier-based method is the Inhomogeneous Wave Correlation (IWC) method, which was proposed by Berthaut et al. [12] and gained extensive use in a variety of applications [13, 14]. The principle of this method is to seek the complex wavenumber corresponding to the maximum of the correlation function between the real displacement field and an inhomogeneous wave field. For two-dimensional structures, the IWC correlation function is a direction-dependent function, leading to the k-space extraction by repeating the algorithm in each direction of interest. It is a robust approach with respect to signal noise and structural perturbations. Tufano et al. [15] have proved its efficiency on metastructures and curved structures. However, the IWC is a non-exact method that converges with a bias. In addition, its performance is limited at low frequencies, as many wavelengths are required within the displacement field to provide a precise estimation. Furthermore, an intricated non-planar wave field will also reduce the accuracy of the method for extracting the imaginary part of the wavenumber [16]. Over the past few decades, some modified versions of the IWC have been developed to improve the performance of the IWC in extracting the imaginary part of k-spaces. In [17], Van Belle et al. propose a modification of the parameterised inhomogeneous wave that takes into account the position of the point load. The inhomogeneous wave is a function of the distance to the point load. The improved method is called the Extended Inhomogeneous Wave Correlation (EIWC) method. Lajili et al. [18, 19] improve the classical IWC by adding a wave in the opposite direction to the inhomogeneous wave. This method is called the Inhomogeneous Wave Correlation Variant (IWC-V) method. While this improvement allows better calculation of complex k-spaces, it still suffers from the same limitations at low frequencies as the classical IWC method. Recently, in his thesis, Tufano [20] replaced the inhomogeneous wave in the correlation with a Green function of the Kirchhoff-Love equation to improve the damping estimation. This idea is combined with the image source method [21] by Fazil in his thesis [22] in the case of a rectangular plate with specific boundary conditions. With enough image sources, the correlation allows a near perfect identification of the damping ratio, even at low frequencies and low damping, but it is limited to isotropic cases. To extend the advantages of Green functions to anisotropic structures, Fazail et al. [23] propose the Green Function Correlation (GFC) method. The correlation is done direction by direction, on one-dimensional parts of the domain, between the Green function and the field. This last method shows a high precision for the complex k-space or damping estimation of composite structures with moderate or high damping. However, it still suffers at low frequencies like most of the IWC methods. In addition, all correlation methods based on the Green function require precise knowledge of the position of the point load.

The Spatial LAplace Transform for COmplex Wavenumber (SLaTCoW) method by Geslain et al. [24], is another wavenumber technique. It makes use of the Laplace transform. The idea is to minimise the L^2 norm of the difference, in the Laplace domain, between the measured signal and a plane wave field parameterised by the complex wavenumbers. This method was developed to find the wavenumbers of one-dimensional fields. An extension to two-dimensional fields, limited to the case of waves propagating in a single direction, has been proposed by Cebrecos et al. [25]. SLaTCoW is efficient for the estimation of complex dispersion characteristics in one-dimensional metamaterial structures [26, 27].

Another class of methods are the Prony-based approaches [28, 29, 30, 31]. Compared to the Fourier-based inverse methods, this category of inverse methods has a high resolution in noiseless conditions and has a good performance at low frequencies. In [32], the High Resolution Wavevector Analysis (HRWA) method was proposed by Margerit et al. to extract the wavenumber space and wavenumber surface of

composite structures. However, the performance of this method is limited by the accuracy of the model order estimation and the complicated sampling manipulation to acquire the local displacement field. A notable Prony-based inverse method is the INverse COnvolution MEthod (INCOME) proposed in [33] by Boukadia et al. This method allows a precise calculation of the complex k-spaces. The method is based on the research of a convolution kernel from which the k-spaces are deduced. Compared to the Fourier-based methods, this method is more accurate and can work at lower frequencies. However, this approach is very sensitive to noise and structural perturbations due to the inherent shortcomings of the Prony method. It also requires the periodic samples as input parameters, resulting in the fact that the periodicity has to be taken into account in the sampling, as explained by Ribeiro et al. in [34]. Moreover, the type of structures has to be known in order to design the convolution kernel in advance.

Other interesting methods, other than those based on Fourier and Prony, can be cited. The image source method proposed by Gunda et al. [21] allows a reconstruction of the harmonic field of rectangular plates excited by a point load with a sum of Hankel functions. This technique was extended to convex polygonal plates with arbitrary boundary conditions by Cuenca et al. [35]. Roozen et al. [36] propose to search the wavenumber by fitting the image source field to the measured field. This technique is limited to convex polygonal plates and the point load must be known exactly, but it allows a precise identification of the wavenumber. Another idea is proposed by Ablitzer et al. [37] in the case of orthotropic structure. They estimate the partial derivative of the harmonic field by finite differences to deduce the directions of orthotropy and then the flexural stiffness properties and the wavenumbers. The previous methods are frequency-domain, however, Morandi et al. [38] gather time-domain methods to estimate the dispersion characteristics. The phase wave velocity is estimated from the time of flight which is calculated from the maximum peak, cross-correlation or kurtosis. The temporal approaches are mostly reserved for the high frequencies.

Although numerous inverse methods are available in the literature, the identification of complex k-spaces at low frequencies or with noisy data, in particular for the imaginary part of complex k-spaces, is still a challenging problem. It is even more problematic in the 2D case. Recently, Li et al. [39] proposed a new approach, the Algebraic Wavenumber Identification (AWI) technique, for the 1D complex structures. This algebraic identification method has been developed based on the algebraic parameters estimator for continuous linear time-invariant systems [40, 41, 42] which has already been applied to vibrating mechanical systems [43, 44]. This wavenumber identification method shows very interesting performances even under stochastic conditions and has been tested on periodic beams. To solve the k-space extraction, a further method has been proposed, namely, the Algebraic K-Space Identification (AKSI) technique [45]. This method was the first to apply a proposed identification procedure to a series of plates. Although this method can extract k-space at a certain degree, it still suffers from the limitation of using 1D scanning points as input. This sampling method can directly lead to difficulties in the accurate extraction of the imaginary part of k-spaces, especially for the low-damping plates. This is mainly because the 1D scanning displacement field lacks enough information of the waves from each direction to reflect the energy propagation.

To overcome the current limitations of the AKSI, this paper proposes a different extension of the AWI method to 2D cases using two-dimensional displacement fields as input parameters, thus renaming it as the AKSI 2D. For the AKSI, a one-dimensional approach is adapted to two-dimensional cases whereas for AKSI 2D, the formulas are developed for two-dimensional cases. From a mathematical point of view, the proposed method introduces two wavenumber variables into the formula and extracts them in a defined characteristic polynomial considering wavenumber components k_x and k_y. This promising method will contribute to the development of the current inverse methods by considering the following aspects:

- This proposed method shows its efficiency and robustness in the calculation of the complex k-spaces under a series of realistic conditions: low frequency, signal noise, and uncertainties from sampling points.

- This proposed method makes it possible to extract complex k-spaces even for the low damping plates. These advantages put the forward of the development of inverse methods in the vibroacoustic field.

- The proposed method extends the AKSI efficiently and has a high potential for solving more vibroa-

coustic inverse problems, such as mechanical parameter estimation.

This paper is structured as follows. Section. 2 presents the formula of the AKSI 2D in detail. Then, Section. 3 shows the validation of the proposed method on analytical fields of isotropic plates and an example of numerical fields from a homogenised orthotropic 2D metastructure, a bi-ribbed plate solved by a finite element method. After that, in Section. 4, the method is applied to experimental displacement fields of a steel plate. Finally, Section. 5 concludes the paper. Three appendices follow the paper, Appendix. A presents the implementation of the IWC and the INCOME in more detail. Appendix. B summarises some of the properties of the Laplace transform used to construct the formulas of the AKSI 2D and Appendix. C describes the numerical implementation of the proposed method.

2. Algebraic K-Space Identification 2D

In order to later perform the comparison with above-mentioned methods, the Algebraic K-Space Identification technique need to be thoroughly presented. This is the purpose of this section with a specific emphasis on two-dimensional wavenumber calculations. The Subsection. 2.1 provides the basic the AKSI 2D formulas for an easy implementation, followed by the detailed explanations for each formula in the Subsection. 2.2. The theory behind them is mostly inspired by the 1D method proposed by Li et al. [39].

2.1. AKSI 2D formulas

Let U be a displacement field on a two-dimensional bounded domain Ω. In particular, $\Omega \subset [0, L_x]\times[0, L_y]$, $L_x, L_y \in \mathbb{R}_+^*$. The field is supposed to be known on some points of a subdomain Ω_w of Ω. The simplest case is when the field is known on a regular rectangular grid on Ω_w: (x_i, y_j) where i ranges from 1 to N_x and j ranges from 1 to N_y. From this displacement field, the AKSI 2D method provides a calculation of the wavenumbers in different directions. The first step is to calculate the coefficients γ by solving the system given by Eqn. (1) for numerous pairs of couples of the grid (x_0, y_0) and (x, y) such that $x_0 < x$ and $y_0 < y$. The system is solved by a least squares method. The formula of the coefficients ϕ_{ik} needed in this equation is presented in Eqn. (2). In these formulas, n_w is the number of plane waves in the field Eqn. (4). The calculation of ϕ_{ik} needs integration calculations that can be done numerically, such as using the trapezoidal method. Their numerical implementation is explained in Appendix. C.

$$\sum_{i=0}^{n_w}\sum_{k=0}^{n_w}\gamma(i,k)\phi_{ik}(x_0,y_0,x,y) = 0, \tag{1}$$

$$\begin{aligned}\phi_{ik}(x_0,y_0,x,y) = \sum_{j=0}^{n_w}\sum_{l=0}^{n_w} &\frac{(-1)^{j+l}(n_w+j)!(n_w+l)!\,(x-x_0)^{n_w-j}\,(y-y_0)^{n_w-l}}{j!(i+j)!(n_w-j)!l!(k+l)!(n_w-l)!} \\ &\times\int_{y_0}^{y}\int_{x_0}^{x}(y-y_1)^{k+l}(x-x_1)^{i+j}U(x_1,y_1)\mathrm{d}x_1\mathrm{d}y_1.\end{aligned} \tag{2}$$

From the knowledge of the values of the coefficient γ, the wavenumber is calculated as a root of a defined polynomial equation Eqn. (3). For each direction θ, the wavenumber calculation requires a resolution of Eqn. (3) but with the same coefficients γ.

$$\Psi(K_\theta) = \sum_{l=0}^{2n_w}(-\mathrm{i}K_\theta)^l\left(\sum_{m=\max(0,l-n_w)}^{\min(l,n_w)}\gamma(n_w-l+m,n_w-m)\cos^{l-m}\theta\sin^m\theta\right). \tag{3}$$

These formulas are explained in the next subsection and are tested for the wavenumbers estimation in the following sections 3 and 4 from the perspective of the analytical, numerical, and experimental study.

2.2. Definition of the formula

First, the field U is approximated by a sum of n_w plane waves with wavenumbers $(k_l)_{1\leq l\leq n_w}$ and in different directions $(\theta_l)_{1\leq l\leq n_w}$.

$$U(x,y)=\sum_{m=1}^{n_w} A_m \mathrm{e}^{-\mathrm{i}k_m(x\cos\theta_m+y\sin\theta_m)}. \tag{4}$$

The 2D Laplace transform is applied to this field and is written as $\mathcal{U}$.

$$\mathcal{U}(s_x,s_y)=\mathcal{L}_y\mathcal{L}_x\left[U(x,y)\right](s_x,s_y)=\sum_{m=1}^{n_w}\frac{A_m}{(s_x+\mathrm{i}k_m\cos\theta_m)(s_y+\mathrm{i}k_m\sin\theta_m)}. \tag{5}$$

The aim is to get a partial differential equation in the Laplace domain. For this reason, the characteristic polynomial with two variables provided in Eqn. (6) is multiplied by $\mathcal{U}$, leading to the Eqn. (7).

$$\Psi(s_x,s_y)=\prod_{m=1}^{n_w}(s_x+\mathrm{i}k_m\cos\theta_m)(s_y+\mathrm{i}k_m\sin\theta_m)=\sum_{i=0}^{n_w}\sum_{k=0}^{n_w}\gamma(i,k)s_x^{n_w-i}s_y^{n_w-k}, \tag{6}$$

$$\mathcal{U}\Psi(s_x,s_y)=\sum_{m=1}^{n_w}\prod_{\substack{l=1\\l\neq m}}^{n_w}(s_x+\mathrm{i}k_l\cos\theta_l)(s_y+\mathrm{i}k_l\sin\theta_l). \tag{7}$$

Eqn. (7) is a polynomial with at most n_w-1 terms in the variables s_x or s_y. Therefore, the following equality is verified for all s_x and s_y.

$$\frac{\partial^{2n_w}\left[\mathcal{U}\Psi\right]}{\partial s_x^{n_w}\partial s_y^{n_w}}(s_x,s_y)=0. \tag{8}$$

Now that a linear partial differential equation is known, it should be developed before using the inverse Laplace transform. First, the following equation is developed by taking Eqn. (6) into Eqn. (8):

$$\frac{\partial^{2n_w}\left[\mathcal{U}\Psi\right]}{\partial s_x^{n_w}\partial s_y^{n_w}}(s_x,s_y)=\sum_{i=0}^{n_w}\sum_{k=0}^{n_w}\gamma(i,k)\frac{\partial^{2n_w}}{\partial s_x^{n_w}\partial s_y^{n_w}}\left[\mathcal{U}s_x^{n_w-i}s_y^{n_w-k}\right]=0. \tag{9}$$

Then the Leibniz formula is used two times on the term $\dfrac{\partial^{2n_w}}{\partial s_x^{n_w}\partial s_y^{n_w}}\left[\mathcal{U}s_x^{n_w-i}s_y^{n_w-k}\right]$. For a given $i\in[\![0,n_w]\!]$, the Leibniz formula gives:

$$\frac{\partial^{n_w}\left[\mathcal{U}s_x^{n_w-i}\right]}{\partial s_x^{n_w}}=\sum_{j=i}^{n_w}\binom{n_w}{j}\binom{n_w-i}{n_w-j}(n_w-j)!s_x^{j-i}\frac{\partial^j\mathcal{U}}{\partial s_x^j}. \tag{10}$$

And so, for $i,\ k\in[\![0,n_w]\!]$:

$$\frac{\partial^{2n_w}\left[\mathcal{U}s_x^{n_w-i}s_y^{n_w-k}\right]}{\partial s_x^{n_w}\partial s_y^{n_w}}=\sum_{j=i}^{n_w}\sum_{l=k}^{n_w}N_{i,j}N_{k,l}s_x^{j-i}s_y^{l-k}\frac{\partial^{j+l}\mathcal{U}}{\partial s_x^j\partial s_y^l}, \tag{11}$$

where $N_{i,j}=\binom{n_w}{j}\binom{n_w-i}{n_w-j}(n_w-j)!$. Based on this, Eqn. (9) can be written as follows:

$$\sum_{i=0}^{n_w}\sum_{k=0}^{n_w}\gamma(i,k)\sum_{j=i}^{n_w}\sum_{l=k}^{n_w}N_{i,j}N_{k,l}s_x^{j-i}s_y^{l-k}\frac{\partial^{j+l}\mathcal{U}}{\partial s_x^j\partial s_y^l}=0. \tag{12}$$

Then this equality is divided by $s_x^{n_w+1}s_y^{n_w+1}$ before applying the inverse Laplace transform and the formula Eqn. (B.5) successively in the direction x and y, so that the transform produces integration and no

derivatives. And by defining the successive integration $\int_x^{(p)} f(x_p) = \int_0^x \int_0^{x_1} \cdots \int_0^{x_{p-1}} f(x_p) \mathrm{d}x_p \ldots \mathrm{d}x_2 \mathrm{d}x_1$, Eqn. (12) becomes, for all (x, y) in Ω:

$$\sum_{i=0}^{n_w} \sum_{k=0}^{n_w} \gamma(i,k) \phi_{ik}(x,y) = 0, \tag{13}$$

with

$$\phi_{ik}(x,y) = \sum_{j=i}^{n_w} \sum_{l=k}^{n_w} N_{i,j} N_{k,l} \int_y^{(n_w+1+k-l)} \int_x^{(n_w+1+i-j)} (-1)^{j+l} x_p^j y_p^l U(x_p, y_p). \tag{14}$$

Next, these formulas are simplified. To avoid the calculation of successive integrations, the following relations are introduced.

$$\int^{(q)} (x_n)^j f(x_n) = \sum_{m=0}^{j} (-1)^m \binom{m+q-1}{q-1} \binom{j}{m} m! x^{j-m} \int^{(m+q)} f(x_n), \tag{15}$$

$$\int^{(q)} f(x_n) = \frac{1}{(q-1)!} \int_0^x (x - x_1)^{q-1} f(x_1) \mathrm{d}x_1, \tag{16}$$

where these two formulas are combined to generate Eqn. (17).

$$\int^{(q)} (x_n)^j f(x_n) = \sum_{r=0}^{n_w} \binom{j}{r} \frac{x^r (-1)^{j-r}}{(q-1)!} \int_0^x (x - x_1)^{j-r+q-1} f(x_1) \mathrm{d}x_1. \tag{17}$$

In particular, in Eqn. (17), the sum of r from 0 to j can be replaced by a sum from 0 to n_w because $j \leq n_w$ and $\binom{j}{r} = 0$ when $r > j$. Replacing the multiple integrations of Eqn. (14) by Eqn. (17), the following equation is obtained:

$$\begin{aligned} \phi_{ik}(x,y) = & \sum_{j=i}^{n_w} \sum_{l=k}^{n_w} \sum_{r=0}^{n_w} \sum_{n=0}^{n_w} M_{i,j,r} M_{k,l,n} x^r y^n \\ & \times \int_0^y \int_0^x (y - y_1)^{n_w+k-n} (x - x_1)^{n_w+i-r} U(x_1, y_1) \mathrm{d}x_1 \mathrm{d}y_1, \end{aligned} \tag{18}$$

where $M_{i,j,r} = N_{i,j} \binom{j}{r} \dfrac{(-1)^r}{(n_w + i - j)!}$. The summations can be switched in Eqn. (18), so that $\sum_{j=i}^{n_w} M_{i,j,r}$ and $\sum_{l=k}^{n_w} M_{k,l,n}$ can be simplified by following formulas.

$$\begin{aligned} \sum_{j=i}^{n_w} M_{i,j,r} &= \sum_{j=i}^{n_w} \binom{n_w}{j} \binom{n_w - i}{n_w - j} (n_w - j)! \binom{j}{r} \frac{(-1)^r}{(n_w + i - j)!} \\ &= \frac{(-1)^r n_w!}{r!(n_w + i - r)!} \sum_{j=i}^{n_w} \binom{n_w - i}{n_w - j} \binom{n_w + i - r}{n_w + i - j} \\ &= \frac{(-1)^r n_w!}{r!(n_w + i - r)!} \frac{(2n_w - r)!}{(n_w - r)! n_w!} \\ &= \frac{(-1)^r (2n_w - r)!}{r!(n_w + i - r)!(n_w - r)!}, \end{aligned} \tag{19}$$

$$\sum_{j=i}^{n_w} M_{i,j,r} = \frac{(-1)^r (2n_w - r)!}{r!(n_w + i - r)!(n_w - r)!}. \tag{20}$$

Based on these simplification operations, the Eqn. (18) becomes:

$$\begin{aligned}\phi_{ik}(x,y) = &\sum_{r=0}^{n_w}\sum_{n=0}^{n_w}\frac{(-1)^{r+n}(2n_w-r)!(2n_w-n)!x^r y^n}{r!(n_w+i-r)!(n_w-r)!n!(n_w+k-n)!(n_w-n)!}\\ &\times\int_0^y\int_0^x (y-y_1)^{n_w+k-n}(x-x_1)^{n_w+i-r}U(x_1,y_1)\mathrm{d}x_1\mathrm{d}y_1,\end{aligned} \tag{21}$$

where two last index r and n are replaced by $r = n_w - j$ and $n = n_w - l$, leading to the following formula:

$$\begin{aligned}\phi_{ik}(x,y) = &\sum_{j=0}^{n_w}\sum_{l=0}^{n_w}\frac{(-1)^{j+l}(n_w+j)!(n_w+l)!x^{n_w-j}y^{n_w-l}}{j!(i+j)!(n_w-j)!l!(k+l)!(n_w-l)!}\\ &\times\int_0^y\int_0^x (y-y_1)^{k+l}(x-x_1)^{i+j}U(x_1,y_1)\mathrm{d}x_1\mathrm{d}y_1.\end{aligned} \tag{22}$$

Up to now, the coefficients ϕ_{ik} are calculated for each point (x, y), these points being the end of each integration. However, all the previous calculations remain valid with the change of coordinates $\tilde{x} = x - x_0$, $\tilde{y} = y - y_0$ and the plane wave field $\tilde{U}$ defined as $\tilde{U}(\tilde{x}, \tilde{y}) = U(\tilde{x} + x_0, \tilde{y} + y_0)$. Therefore, a definition of the terms ϕ_{ik} that takes into account starting points of the integrations other than $(0, 0)$, can replace Eqn. (22). For all (x_0, y_0) and (x, y) in Ω, such that $x_0 < x$ and $y_0 < y$, $\phi_{ik}(x_0, y_0, x, y)$ is defined in Eqn. (23).

$$\begin{aligned}\phi_{ik}(x_0,y_0,x,y) = &\sum_{j=0}^{n_w}\sum_{l=0}^{n_w}\frac{(-1)^{j+l}(n_w+j)!(n_w+l)!\,(x-x_0)^{n_w-j}\,(y-y_0)^{n_w-l}}{j!(i+j)!(n_w-j)!l!(k+l)!(n_w-l)!}\\ &\times\int_{y_0}^y\int_{x_0}^x (y-y_1)^{k+l}(x-x_1)^{i+j}U(x_1,y_1)\mathrm{d}x_1\mathrm{d}y_1.\end{aligned} \tag{23}$$

And Eqn. (13) is valid for each pair of couples (x_0, y_0) and (x, y) when $x_0 < x$ and $y_0 < y$:

$$\sum_{i=0}^{n_w}\sum_{k=0}^{n_w}\gamma(i,k)\phi_{ik}(x_0,y_0,x,y) = 0. \tag{24}$$

These two formulas correspond to Eqn. (1) and (2). In this way, the quantity of data for the calculation of the coefficients γ is greatly increased and the importance of each point of the domain is more balanced. Then, the coefficients γ are a non-zero solution of a linear system. For each point of the mesh, Eqn. (24) is evaluated. If the mesh is rectangular, the system is the following one:

$$\mathbf{HX = 0,} \tag{25}$$

with:

$$\mathbf{H_p} = \begin{bmatrix} \phi_{0p}(x_1,y_1,x_2,y_2) & \dots & \phi_{n_wp}(x_1,y_1,x_2,y_2)\\ \phi_{0p}(x_1,y_1,x_3,y_2) & \dots & \phi_{n_wp}(x_1,y_1,x_3,y_2)\\ \vdots & \ddots & \vdots\\ \phi_{0p}(x_1,y_1,x_{N_x},y_2) & \dots & \phi_{n_wp}(x_1,y_1,x_{N_x},y_2)\\ \phi_{0p}(x_1,y_1,x_2,y_3) & \dots & \phi_{n_wp}(x_1,y_1,x_2,y_3)\\ \vdots & & \vdots\\ \phi_{0p}(x_1,y_1,x_{N_x},y_{N_y}) & \dots & \phi_{n_wp}(x_1,y_1,x_{N_x},y_{N_y})\\ \phi_{0p}(x_2,y_1,x_3,y_2) & \dots & \phi_{n_wp}(x_2,y_1,x_3,y_2)\\ \vdots & & \vdots\\ \phi_{0p}(x_{N_x-1},y_{N_y-1},x_{N_x},y_{N_y}) & \dots & \phi_{n_wp}(x_{N_x-1},y_{N_y-1},x_{N_x},y_{N_y}) \end{bmatrix}, \tag{26}$$

$$\mathbf{H} = \begin{bmatrix}\mathbf{H_0} & \mathbf{H_1} & \dots & \mathbf{H_{n_w}}\end{bmatrix}, \tag{27}$$

and

$$\mathbf{X} = \begin{bmatrix} \gamma(0,0) \\ \gamma(1,0) \\ \vdots \\ \gamma(n_w,0) \\ \gamma(0,1) \\ \vdots \\ \gamma(n_w,n_w) \end{bmatrix}. \tag{28}$$

This system is solved in the least squares sense Eqn. (29).

$$\begin{cases} \mathbf{X} = \underset{\mathbf{Y}\in\mathbb{C}^{n_w^2}}{\operatorname{argmin}} \mathbf{Y}^*\mathbf{H}^*\mathbf{H}\mathbf{Y}, \\ \|\mathbf{X}\|_2 = 1, \end{cases} \tag{29}$$

$\bullet^*$ is the Hermitian transpose. $\mathbf{H}^*\mathbf{H}$ is a Hermitian matrix, so by the Fischer–Courant min-max principle [46], the minimum of $\mathbf{Y}^*\mathbf{H}^*\mathbf{H}\mathbf{Y}$ with $\|\mathbf{Y}\|_2 = 1$ is the smallest eigenvalue of $\mathbf{H}^*\mathbf{H}$. Therefore, $\mathbf{X}$ is calculated as a numerical approximation of an eigenvector associated with the smallest eigenvalue of $\mathbf{H}^*\mathbf{H}$.

Finally, from the knowledge of the coefficients γ, the characteristic polynomial can be reconstructed. To get a one-variable polynomial, variable changes are considered, with K_θ the indeterminate and θ a selected direction of study.

$$\begin{aligned} s_x &= -\mathrm{i}K_\theta \cos\theta, \\ s_y &= -\mathrm{i}K_\theta \sin\theta. \end{aligned} \tag{30}$$

Therefore, Eqn. (6) becomes:

$$\begin{aligned} \Psi(K_\theta) &= \sum_{i=0}^{n_w}\sum_{k=0}^{n_w} \gamma(i,k)\left(-\mathrm{i}K_\theta\right)^{2n_w-k-i} \cos^{n_w-i}\theta \sin^{n_w-k}\theta \\ &= \sum_{l=0}^{2n_w} (-\mathrm{i}K_\theta)^l \left(\sum_{m=\max(0,l-n_w)}^{\min(l,n_w)} \gamma(n_w-l+m, n_w-m) \cos^{l-m}\theta \sin^m\theta \right). \end{aligned} \tag{31}$$

This formula corresponds to the Eqn. (3). The complex wavenumber in the direction θ is a root of this polynomial. To obtain a k-space, a search for roots is performed at each value of the angle θ.

2.3. Specific cases

In practice, in some specific situations, the implementation of the proposed method can be modified to gain precision or efficiency.

Firstly, k-spaces present some symmetries and some coefficients are not necessarily to be taken into account. For a given direction θ:

$$k_\theta = k_{\pi+\theta}. \tag{32}$$

Thus, Eqn. (31) in the direction $\pi+\theta$ can be obtained by the following formula:

$$\Psi(K_{\pi+\theta}) = \sum_{i=0}^{n_w}\sum_{k=0}^{n_w} \gamma(i,k)\left(-\mathrm{i}K_{\pi+\theta}\right)^{2n_w-k-i} (-1)^{2n_w-k-i} \cos^{n_w-i}\theta \sin^{n_w-k}\theta. \tag{33}$$

And by adding Eqn. (31) with Eqn. (33) and Eqn. (32), the characteristic polynomial becomes:

$$\begin{aligned}\Psi(K_\theta) &= \sum_{i=0}^{n_w}\sum_{\substack{k=0\\ i \text{ and } k \text{ of the same parity}}}^{n_w} \gamma(i,k)\left(-\mathrm{i}K_\theta\right)^{2n_w-k-i}\cos^{n_w-i}\theta\sin^{n_w-k}\theta \\ &= \sum_{l=0}^{n_w}(-K_\theta^2)^l\left(\sum_{m=\max(0,2l-n_w)}^{\min(2l,n_w)}\gamma(n_w-2l+m,n_w-m)\cos^{2l-m}\theta\sin^m\theta\right).\end{aligned} \tag{34}$$

This means that $\gamma(i,k)$ is not considered if i and k are not of the same parity. Then, if the studied field is supposed orthotropic, other symmetries can be added.

$$k_\theta = k_{\pi+\theta} = k_{-\theta} = k_{\pi-\theta}. \tag{35}$$

Following the same reasoning as before, it comes that $\gamma(i,k)$ is not considered if $n_w - i$ or $n_w - k$ is odd. The characteristic polynomial Eqn. (3) is replaced by Eqn. (36).

$$\begin{aligned}\Psi(K_\theta) &= \sum_{i=0}^{\left\lfloor\frac{n_w}{2}\right\rfloor}\sum_{k=0}^{\left\lfloor\frac{n_w}{2}\right\rfloor}\gamma(n_w-2i,n_w-2k)\left(-K_\theta^2\right)^{k+i}\cos^{2i}\theta\sin^{2k}\theta \\ &= \sum_{l=0}^{n_w}(-K_\theta^2)^l\left(\sum_{m=\max\left(0,l-\left\lfloor\frac{n_w}{2}\right\rfloor\right)}^{\min\left(l,\left\lfloor\frac{n_w}{2}\right\rfloor\right)}\gamma(n_w-2(l-m),n_w-2m)\cos^{2(l-m)}\theta\sin^{2m}\theta\right).\end{aligned} \tag{36}$$

And Eqn. (1) is replaced by Eqn. (37).

$$\sum_{i=0}^{\left\lfloor\frac{n_w}{2}\right\rfloor}\sum_{k=0}^{\left\lfloor\frac{n_w}{2}\right\rfloor}\gamma(n_w-2i,n_w-2k)\phi_{n_w-2i,n_w-2k}(x_0,y_0,x,y) = 0. \tag{37}$$

The results obtained with the symmetries taken into account seem to be better and make the method more robust.

Then, if the field has a singularity in it with a known location, such as a point load, the application of the method to calculate k-space cannot work well. To solve this problem, the points near the singularity must not be used in the calculation of the coefficients ϕ_{ik}. Let Ω_M be a subdomain of Ω centred on the singularity. If this subdomain overlaps with the area of integration between (x_0, y_0) and (x, y) (so if Eqn. (38) is verified), then $\phi_{ik}(x_0, y_0, x, y)$ is ignored.

$$[x_0, x] \times [y_0, y] \cap \Omega_m \neq \emptyset. \tag{38}$$

In this way, the singularity does not affect the calculated wavenumbers.

And finally, when dealing with large-scale problems, the computational cost can be high, with all the multiple measurement points in a large-scale 2D grid as input. However, the AKSI 2D has a flexible computational cost depending on the number of measurements used. For large-scale plates, three solutions can be applied to reduce the computational cost:

- Not every possible 4-uplet (x_0, x, y_0, y) needs to be used, and a reduced 2D grid can be considered as input. In particular, at low frequencies, with large wavelengths, a rougher grid may be sufficient for accurate k-space calculations. Conversely, at high frequencies, with small wavelengths, the overall size can sometimes be reduced.

- The computation of the Eqn. (2) can be optimised, as explained in Appendix. C by using previous calculations to simplify the next ones and thus reduce the computational time.
- Using only the points far from the excitation and boundary can also reduce the evanescent wave influence but also reduce the computational time for the AKSI 2D.

3. Analytical and numerical validations

The method is now tested on fields calculated analytically and numerically. Comparisons with the IWC [12] and the INCOME [33] are provided. To compare the methods, an example of an isotropic plate and an example of an orthotropic plate are presented. The robustness to noise and uncertainties is also examined.

3.1. Analytical model of isotropic plate

The first plate is an isotropic plate that follows the Kirchhoff Love plate equation Eqn. (39) [47].

$$D\Delta^2 u - \omega^2 \Lambda u = f. \tag{39}$$

The mechanical properties of the steel are chosen. In particular, the geometrical properties of this plate are chosen to match the experimental case presented in Section. 4.

3.1.1. Steel plate

The steel plate has the following properties, Young modulus $E = 210\,\text{GPa}$, volume mass $\rho = 7900\,\text{kg/m}^3$ and a Poisson ratio $\nu = 0.3$. A damping of $\eta = 2\%$ is added to the Young Modulus $\tilde{E} = E(1 + \mathrm{i}\eta)$. The damping ratio of steel is too low to have a clear measure of the imaginary part of the wavenumbers, that is why the value chosen in the analytical model is taken higher: at 2%. But it is still a case of low damping.

The plate is rectangular, $L_x = 0.95\,\text{m}$, $L_y = 0.6\,\text{m}$ with a thickness $d = 0.002\,\text{m}$. The following quantities are calculated from the previous: the surface mass $\Lambda = d\rho$, the flexural inertia modulus $I = \dfrac{d^3}{12}$, the bending rigidity $D = \dfrac{\tilde{E}}{1-\nu^2} I$ and the wavenumber k such that:

$$k^4 = \omega^2 \frac{\Lambda}{D}. \tag{40}$$

The steel plate has a point load at (x_s, y_s) and simply supported conditions at the boundaries. The analytical solution calculated by modal decomposition in this case is the following one Eqn. (41).

$$u_{analytic}(x,y) = \sum_{n=0}^{+\infty}\sum_{m=0}^{+\infty} \frac{4 \sin\left(\frac{n\pi x_s}{L_x}\right) \sin\left(\frac{m\pi y_s}{L_y}\right) \sin\left(\frac{n\pi x}{L_x}\right) \sin\left(\frac{m\pi y}{L_y}\right)}{L_x L_y \left(D\left(\left(\frac{n\pi}{L_x}\right)^2 + \left(\frac{m\pi}{L_y}\right)^2\right)^2 - \omega^2 \Lambda\right)}. \tag{41}$$

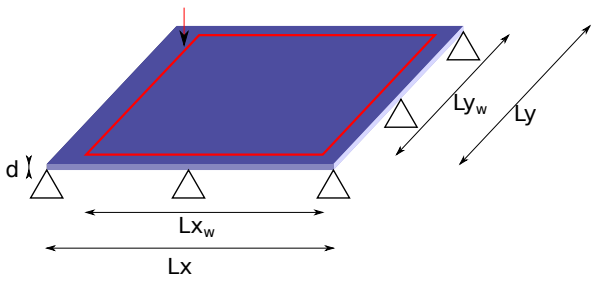

Figure 1: Schema of the plate.

3.1.2. Damping loss factor

From the dispersion characteristics of a displacement field, the group velocity $c_g = \dfrac{\partial \omega}{\partial \mathfrak{Re}(k)}$ and the phase velocity $c_\varphi = \dfrac{\omega}{\mathfrak{Re}(k)}$ can be deduced. Therefore, the damping loss factor can be estimated as a function of the angular frequency and the direction, [23, 48, 49]:

$$\eta(\omega, \theta) = -2 \frac{\mathfrak{Im}(k_\theta)}{\mathfrak{Re}(k_\theta)} \frac{c_g}{c_\varphi}. \tag{42}$$

Manconi et al. [50] propose an average definition of the damping loss factor using the angular modal density to take into account the non-isotropic cases. The modal density is given Eqn. (43), where S is the area of the structure and the average loss factor is given by Eqn. (44).

$$n(\omega, \theta) = \frac{S}{\pi^2} \frac{\mathfrak{Re}(k_\theta(\omega))}{c_g(\omega, \theta)}, \tag{43}$$

$$\bar{\eta}(\omega) = \frac{\displaystyle\int_0^{2\pi} \eta(\omega, \theta) n(\omega, \theta) \mathrm{d}\theta}{\displaystyle\int_0^{2\pi} n(\omega, \theta) \mathrm{d}\theta} = \frac{\displaystyle\int_0^{2\pi} \eta(\omega, \theta) \frac{\mathfrak{Re}(k_\theta(\omega))}{c_g(\omega, \theta)} \mathrm{d}\theta}{\displaystyle\int_0^{2\pi} \frac{\mathfrak{Re}(k_\theta(\omega))}{c_g(\omega, \theta)} \mathrm{d}\theta}. \tag{44}$$

Since the calculation of the group velocity requires an approximation of a derivative, a smoothing is applied to wavenumbers in the procedure of damping loss factor estimation.

3.1.3. k-space methods comparison

The k-space methods are tested and compared with the analytical solution given by Eqn. (40), in this case, on a frequency band from 3.125 Hz to 2500 Hz. Since an isotropic structure is a particular case of orthotropy, the AKSI 2D method adapted to orthotropic structures, based on the formulas Eqn. (2), (37) and (36) is used. The dispersion relations are shown in Fig. 2 and k-spaces at the frequencies 250 Hz, 1250 Hz and 2500 Hz are shown in Fig. 3. Moreover, using Eqns. (42) and (44), the average loss factor is estimated and compared to the initial value of 0.02%.

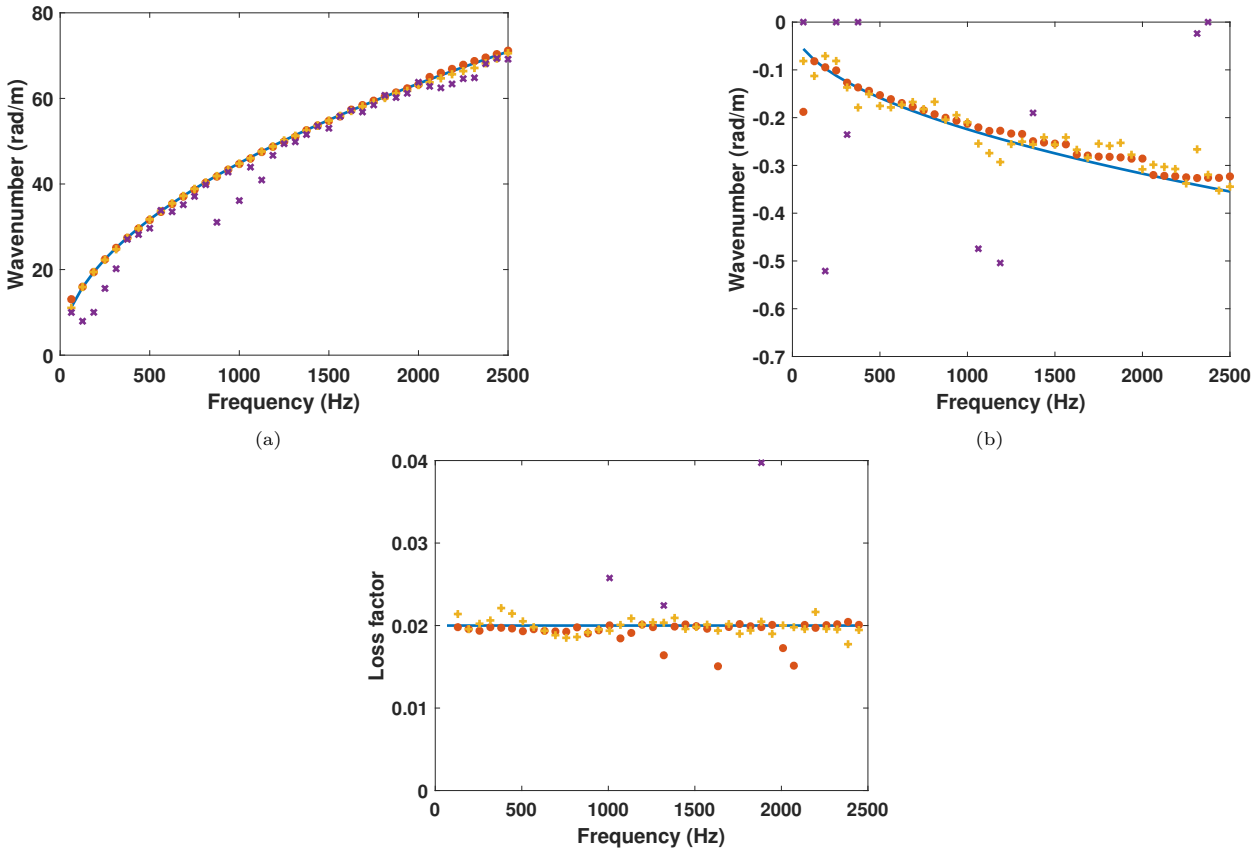

Figure 2: Dispersion relation in the direction 0 rad of the steel plate: (a) real part, (b) imaginary part and (c) average damping loss factor. Analytical solution (−), the AKSI 2D (•) the INCOME (+) and the IWC (x).

All the three methods, the IWC, the INCOME and the AKSI 2D give a good real part of the wavenumbers at each frequency and direction Figs. 2a, 3a, 3b and 3c. However, for the imaginary part, the AKSI 2D seems to be as effective as the INCOME and much better than the IWC in this frequency range Figs. 2b, 3d, 3e and 3f. And for the damping loss factor, Fig. 2c, the values estimated based on the AKSI 2D are almost as precise as those based on the INCOME, except for a few frequencies. In terms of computational efficiency, the INCOME is by far the best of the three methods. It is a very fast algorithm based on a linear Prony principle that only requires solving several sample linear equations. The whole process does not require the calculation of integrals of the signals. The two other methods, the IWC and the AKSI 2D are more time-consuming. The fact that the IWC is time-consuming has already been discussed in the literature, in the work of Margerit et al. [51]. It deals with the search of the maximum on a 2D set, done by evaluation or by an iterative process and each evaluation requires an integral calculation. The time-consuming computation of the AKSI 2D also results from the calculation of integrations of the signal. These are given Eqn. (2), where the measurement coordinate pairs (x_0, y_0) and (x, y) determine the number of measurement points involved in this integration. Thus, the computational cost of the AKSI 2D depends on the number of measured points used in the above equation. However, the AKSI 2D has some flexibility in the number of measured points considered, as explained in Subsection. 2.3.

3.2. Robustness to noise and position uncertainties

The next stage of the comparative evaluation for the AKSI 2D method focuses on their relative robustness. The test cases remain the same as before, namely the steel plate. Added noise and position uncertainty cases are considered here.

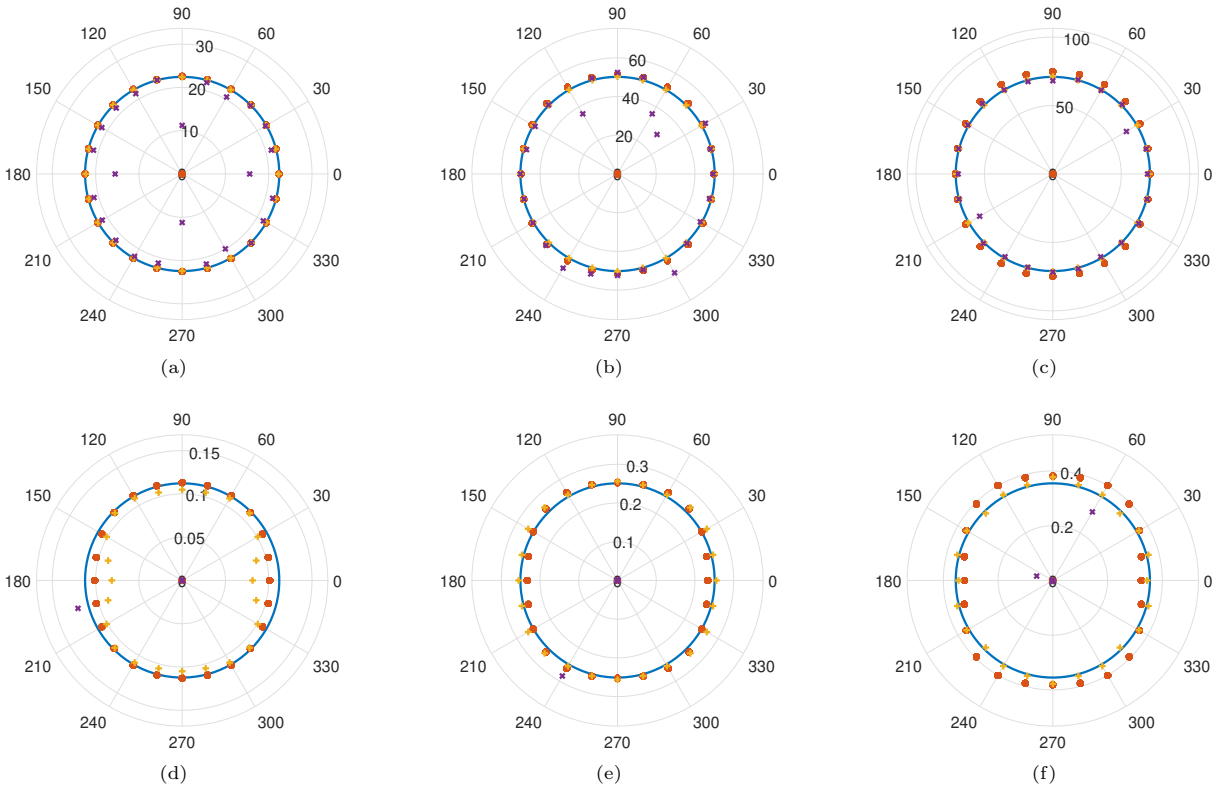

Figure 3: Real and imaginary parts of k-spaces of the steel plate at three frequencies. Analytical solution (−), the AKSI 2D (•) the INCOME (+) and the IWC (x). (a) real part at 250 Hz, (b) real part at 1250 Hz, (c) real part at 2500 Hz, (d) imaginary part at 250 Hz, (e) imaginary part at 1250 Hz and (f) imaginary part at 2500 Hz.

The noise is added to the fields calculated with Eqn. (41) and the noise follows a uniform law.

$$\tilde{u}(x_n, y_m) = u(x_n, y_m) + \epsilon_{n,m}, \tag{45}$$

with $\epsilon \rightsquigarrow \mathcal{U}(-a, a)$, and a chosen such that $SNR = \dfrac{\|u\|_{L^2}}{\|\epsilon\|_{L^2}} = 20$.

The extracted dispersion curves and complex k-spaces are shown in Figs. 4 and 5. From these figures, it can be seen that while the real part of the wavenumbers is well calculated by the three methods in most of the cases, the AKSI 2D method can provide more acceptable results for the imaginary part and the average damping loss estimation with added noise. Comparing the imaginary part and damping loss factor calculated by the AKSI 2D from fields with added noise Fig. 4 and with perfect field Fig. 2, it is seen that the noise has an impact on the calculations. However, the trend is still good. The same can be said for the imaginary part of the k-spaces, Figs. 3 and 5. The imaginary part of the k-spaces calculated with the AKSI 2D with added noise has more variability with the direction than without noise, but the values are still around the analytical ones.

To compare more in detail the effect of noise on the k-space calculation, a study of the variations of the relative error on the real and imaginary parts of the k-spaces function of the SNR is provided in Fig. 6. The test field is the analytical solution of the Kirchhoff-Love equation at the frequency 250 Hz. Each value of SNR has been tested 48 times with a different random draw of noise. In this figure, it can be seen that the IWC is the least accurate method, but is very little affected by the noise. The behaviour of the measurements made by the AKSI 2D and the INCOME are very different, even for a fixed value of SNR, the effect on the INCOME is very variable. For the lowest values of noise, so the highest values of SNR presented, many of the k-spaces calculated by the INCOME have a relative error above 0.1 for the real part

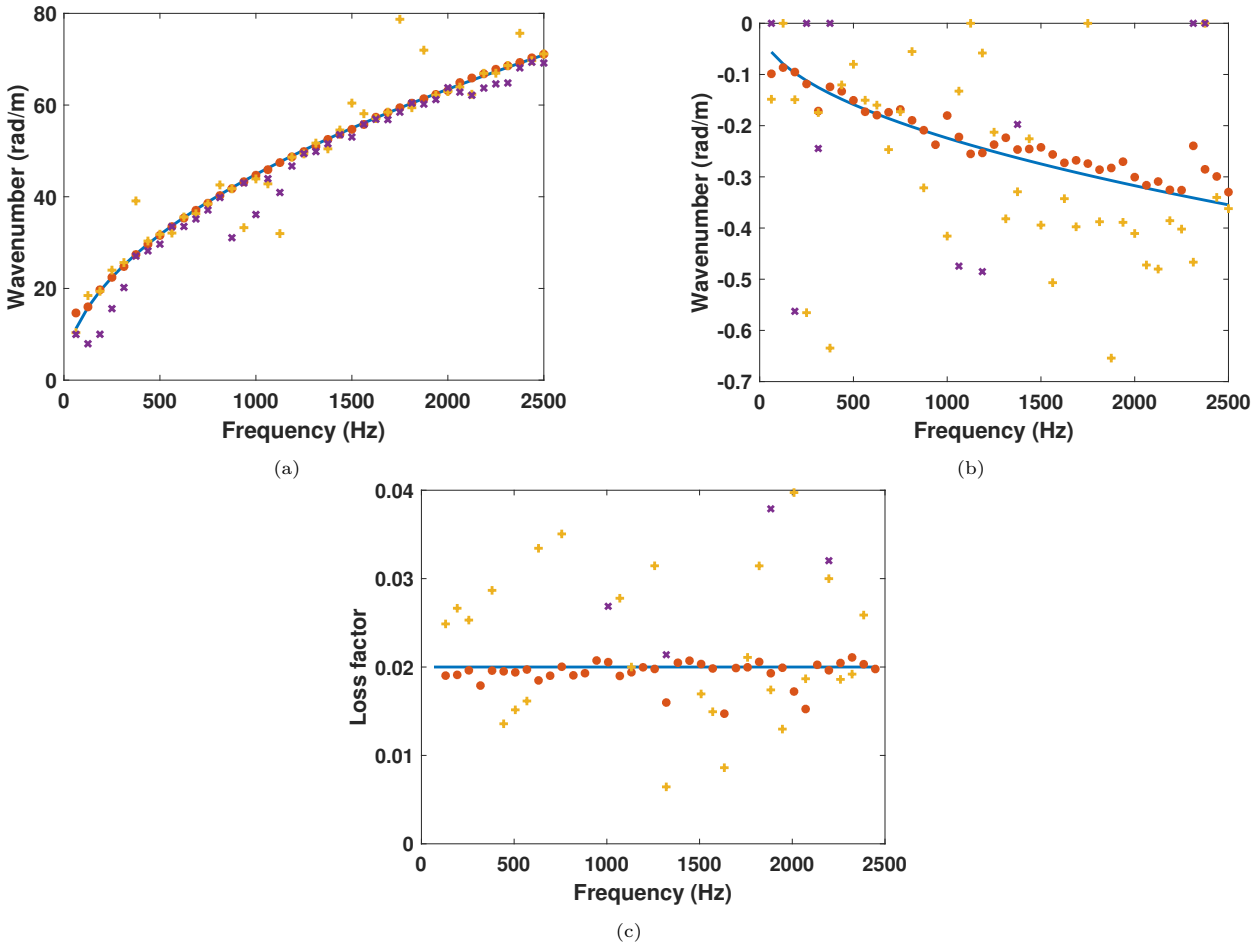

Figure 4: Dispersion relation in the direction 0 rad of the steel plate with an added noise, $SNR = 20$: (a) real part, (b) imaginary part and (c) average damping loss factor. Analytical solution (−), the AKSI 2D (•) the INCOME (+) and the IWC (x).

and above 1 for the imaginary part. To observe a decrease in the relative error with this method, the SNR has to be far higher. Conversely, the AKSI 2D appears to be much more robust. The results from this method show a decrease in the relative error as the SNR increases. The relative error based on the AKSI 2D at very high noise is better than those based on the INCOME and the IWC for the real part. For the imaginary part, the relative error becomes acceptable well before the other methods. Moreover, a noise of SNR above 30 has almost no effect on the calculation of the real part of the k-space by the AKSI 2D. For the imaginary part, this limit is around 100.

The same type of study is conducted with positional uncertainties. The fields are generated so that

$$\bar{u}(x_n, y_m) = u(x_n + \delta x_{n,m}, y_m + \delta y_{n,m}), \tag{46}$$

δx and δy follow uniform laws: $\delta x \rightsquigarrow \mathcal{U}\left(-\frac{\Delta x}{4}, \frac{\Delta x}{4}\right)$ and $\delta y \rightsquigarrow \mathcal{U}\left(-\frac{\Delta y}{4}, \frac{\Delta y}{4}\right)$ where Δx and Δy are the spatial step of the discretisation in the direction x and y in the perfect case. Eqn. (41) is used to calculate $\bar{u}$. The resulting dispersion curves and complex k-spaces are shown in Figs. 7 and 8.

The conclusions of Figs. 7 and 8 for wavenumbers extraction on fields with position uncertainties are the same as with added noise. The real parts calculated by the AKSI 2D are at least as good as those calculated with other methods and are close to the analytical values. The imaginary part of the wavenumbers calculated

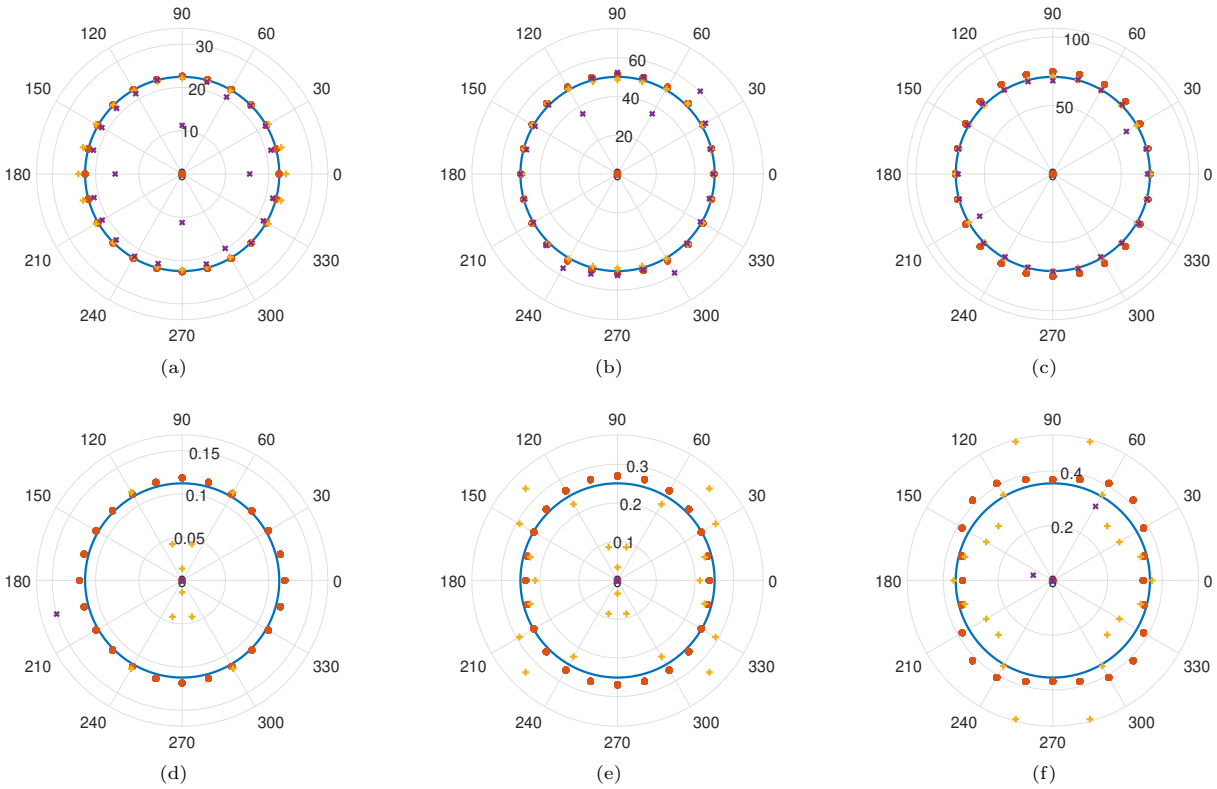

Figure 5: Real and imaginary parts of k-spaces of the steel plate at three frequencies with an added noise with $SNR = 20$. Analytical solution (−), the AKSI 2D (•) the INCOME (+) and the IWC (x). (a) real part at 250 Hz, (b) real part at 1250 Hz, (c) real part at 2500 Hz, (d) imaginary part at 250 Hz, (e) imaginary part at 1250 Hz and (f) imaginary part at 2500 Hz.

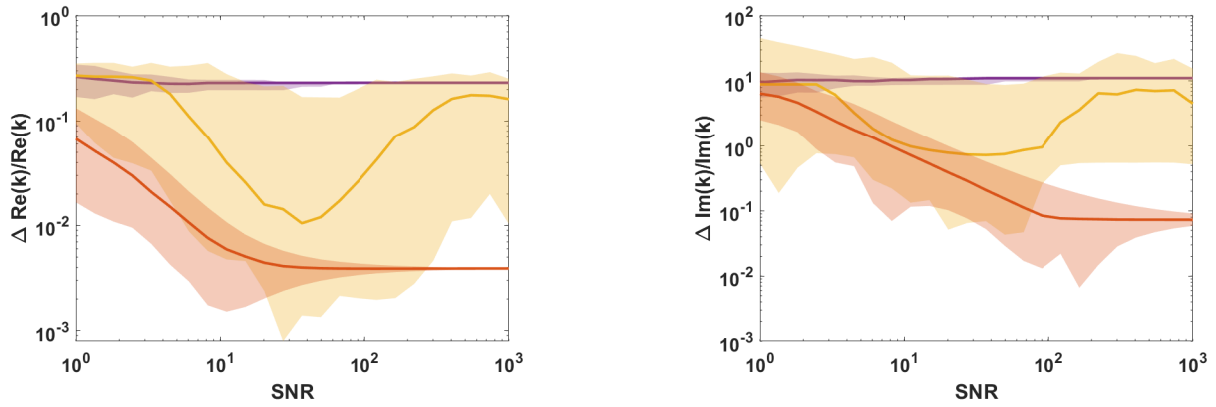

(a) (b)

Figure 6: Relative error in the identification of the k-space as a function of the SNR. Comparison between the IWC (−), the INCOME (−) and the AKSI 2D (−): (a) real part, (b) imaginary part. The area is coloured between the highest and lowest value of relative error at each SNR value. The full line is the median of the relative error at each SNR value.

by the AKSI 2D is a little perturbed but is still close to the analytical values when the results of the INCOME

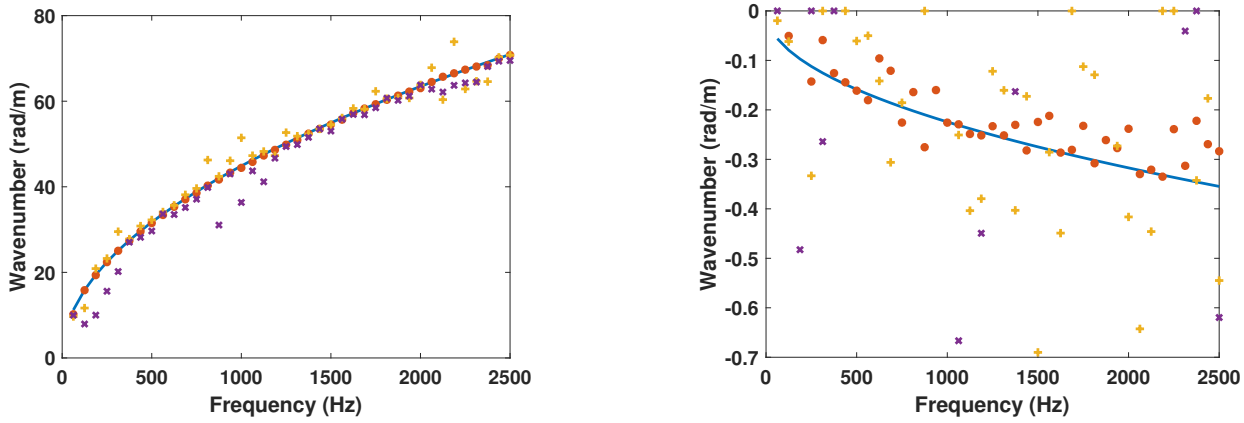

(a) (b)

Figure 7: Dispersion relation in the direction 0 rad of the steel plate with position uncertainties: (a) real part, (b) imaginary part. Analytical solution (−), the AKSI 2D (•) the INCOME (+) and the IWC (x).

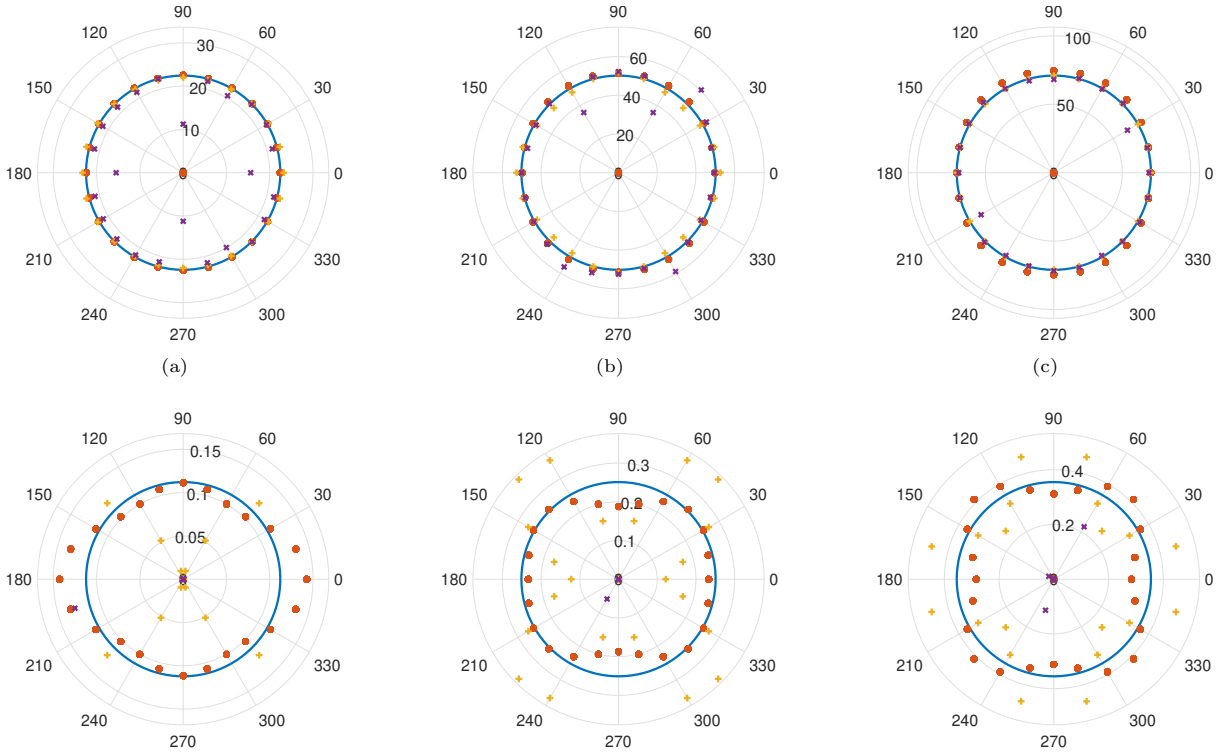

(a) (b) (c) (d) (e) (f)

Figure 8: Real and imaginary parts of k-spaces of the steel plate at three frequencies with position uncertainties. Analytical solution (−), the AKSI 2D (•) the INCOME (+) and the IWC (x). (a) real part at 250 Hz, (b) real part at 1250 Hz, (c) real part at 2500 Hz, (d) imaginary part at 250 Hz, (e) imaginary part at 1250 Hz and (f) imaginary part at 2500 Hz.

and the IWC are not accurate.

Now that the advantage of the AKSI 2D method has been demonstrated on an isotropic case with and without noise or uncertainties, a case of an orthotropic structure is presented.

3.3. Numerical model of a bidirectional ribbed plate

A bidirectional ribbed plate is a periodic structure, illustrated in Fig. 9, made of a plate to which two perpendicular rows of stiffeners have been added. Since the beam grid of the stiffeners is supposed to be stiffer than the plates put between them, the dynamics of the stiffeners is dominant in the structure. That is why this metastructure presents a multiscale dynamic. The AKSI 2D method is tested on this type of structure to verify its efficiency on complex structures. Boutin et al. [52] have provided an analytical model of the flexural behaviour of this type of structure that will serve as a reference. It is a model of an equivalent orthotropic plate obtained from an asymptotic homogenisation process.

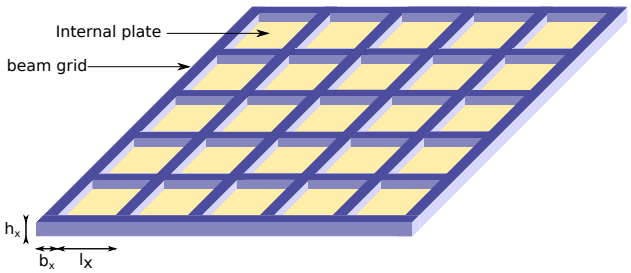

Figure 9: Example of a bidirectional ribbed plate of 5 by 5 cells.

This model is a 4th-order partial differential equation which result from the enrichment of an orthotropic plate equivalent to a beam grid, as the stiffeners are dominant compared to the plates in the global dynamics.

Let h_j and b_j be respectively the height and the width of the stiffeners of the direction j. j being x or y. l_j is the contact length of the stiffeners with an inner plate. About the mechanical properties of the stiffeners: E_j, ν_j and ρ_j are respectively the Young Modulus, the Poisson ratio and the volume mass. A damping is added as an imaginary part of the Young modulus. η is the damping ratio and $\tilde{E}_j = E_j(1+\mathrm{i}\eta)$. From these parameters, some important quantities can be deduced: the bending inertia $I_j = \dfrac{b_j h_j^3}{12}$, the torsional modulus $G_j = \dfrac{\tilde{E}_j}{2(1+\nu_j)}$, the torsional inertia $\mathcal{I}_j = \dfrac{b_j}{2}\left(\dfrac{h_j}{2}\right)^3\left(\dfrac{16}{3} - 3.36\dfrac{h_j}{b_j}\left(1 - \dfrac{h_j^4}{12b_j^4}\right)\right)$, the linear mass $\Lambda_j = \rho_j b_j h_j$ and the torsional constant, $\rho_j J_j = \rho_j h_j b_j \dfrac{b_j^2 + h_j^2}{12}$. The torsional inertia of a beam of rectangular section comes from [53]. In addition to these parameters, the properties of the internal plates must be defined. All the plates have the same properties and are clamped to the beam grid. l_x, l_y are the side lengths and d is the width. E_p is the Young modulus, ν_p the Poisson ratio and ρ_p the volume mass. From these parameters, the following ones are calculated: the surface mass $\Lambda'_p = \rho_p d$, the bending inertia $I_p = \dfrac{d^3}{12}$ and the modified Young modulus $E'_p = \dfrac{E_p(1+\mathrm{i}\eta)}{1-\nu_p^2}$.

With these parameters, the equation of the model of an orthotropic plate equivalent to a bi-ribbed plate proposed is Eqn. (47).

$$\begin{aligned}\frac{\tilde{E}_x I_x}{l_y}\frac{\partial^4 u}{\partial x^4} + \frac{\tilde{E}_y I_y}{l_x}\frac{\partial^4 u}{\partial y^4} + \left(\frac{G_x \mathcal{I}_x}{l_y} + \frac{G_y \mathcal{I}_y}{l_x}\right)\frac{\partial^4 u}{\partial x^2 \partial y^2} \\ +\omega^2\left(\frac{\rho_y J_y}{l_x}\frac{\partial^2 u}{\partial x^2} + \frac{\rho_x J_x}{l_y}\frac{\partial^2 u}{\partial y^2}\right) + \left(K^{bc}_{\omega_x}\frac{\partial u}{\partial x} + K^{bc}_{\omega_y}\frac{\partial u}{\partial y}\right) \\ = \omega^2\left(\frac{\Lambda_x}{l_y} + \frac{\Lambda_y}{l_x} + \Lambda'_p\left\langle\phi^{bc}_\omega\right\rangle\right)u.\end{aligned} \tag{47}$$

The different terms of this equation can be interpreted. The model of a beam grid contains the flexural rigidity of the stiffeners in the two directions $\dfrac{\tilde{E}_x I_x}{l_y}\dfrac{\partial^4 u}{\partial x^4}$ and $\dfrac{\tilde{E}_y I_y}{l_x}\dfrac{\partial^4 u}{\partial y^4}$, a torsional rigidity term

$\left(\frac{G_x\mathcal{I}_x}{l_y}+\frac{G_y\mathcal{I}_y}{l_x}\right)\frac{\partial^4 u}{\partial x^2\partial y^2}$, a rotational inertia term $\omega^2\left(\frac{\rho_y J_y}{l_x}\frac{\partial^2 u}{\partial x^2}+\frac{\rho_x J_x}{l_y}\frac{\partial^2 u}{\partial y^2}\right)$. There is an unconventional torque term $\left(K^{bc}_{\omega_x}\frac{\partial u}{\partial x}+K^{bc}_{\omega_y}\frac{\partial u}{\partial y}\right)$ but it does not appear here as the plates are clamped on the beam grid. And finally, there is an inertia term $\omega^2\left(\frac{\Lambda_x}{l_y}+\frac{\Lambda_y}{l_x}+\Lambda'_p\left\langle\phi^{bc}_\omega\right\rangle\right)u$. This last term adds to the mass of the beam grid, an added mass term $\Lambda'_p\left\langle\phi^{bc}_\omega\right\rangle$ that takes into account the effect of the dynamics of the internal plates. The non-conventional term $\left\langle\phi^{bc}_\omega\right\rangle$ is the mean of the out-of-plane displacement on an internal plate with a unitary displacement at its boundaries. It is a frequency dependent term that depends on the boundary conditions of the internal plates. In the case of square plates ($l_x = l_y$), which are clamped on all sides, there is no analytical formula. Therefore the square plate is approximated by a circular plate of radius r to be determined. With this approximation:

$$\left\langle\phi^{CCCC}_\omega\right\rangle = \frac{4}{\delta r}\frac{I_1(\delta r)J_1(\delta r)}{I_1(\delta r)J_0(\delta r)+I_0(\delta r)J_1(\delta r)}, \tag{48}$$

where $\delta^4 = \frac{\omega^2\Lambda_p}{E'_p I_p} = (2\pi f)^2\frac{\Lambda_p(1-\nu_p^2)}{E_p\,(1+\mathrm{i}\eta)\,I_p}$, J_0, J_1 are the Bessel functions of the first kind, I_0, I_1 are modified Bessel functions of the first kind and $r = 0.532\,l$. From Eqn. (47) the analytical dispersion relation is defined by replacing the solution u by a plane wave in the direction θ, $U(x,y) = \mathrm{e}^{\mathrm{i}k_\theta(x\cos\theta+y\sin\theta)}$:

$$\begin{aligned} &k_\theta^4\left(\frac{\tilde{E}_x I_x}{l_y}\cos^4\theta+\frac{\tilde{E}_y I_y}{l_x}\sin^4\theta+\left(\frac{G_x\mathcal{I}_x}{l_y}+\frac{G_y\mathcal{I}_y}{l_x}\right)\cos^2\theta\sin^2\theta\right)\\ -&k_\theta^2\omega^2\left(\frac{\rho_y J_y}{l_x}\cos^2\theta+\frac{\rho_x J_x}{l_y}\sin^2\theta\right)=\omega^2\left(\frac{\Lambda_x}{l_y}+\frac{\Lambda_y}{l_x}+\Lambda'_p\left\langle\phi^{bc}_\omega\right\rangle\right)u. \end{aligned} \tag{49}$$

The stiffeners are supposed to be the same in the x and the y directions and made of aluminium and the plates are made of plexiglass. In addition, a damping of $\eta = 5\%$ is added to the Young modulus as an imaginary part. Table. 1 contains the properties of the stiffener and Table. 2 contains those of the internal plate.

Parameter:	h_x, h_y	b_x, b_y	E_x, E_y	ν_x, ν_y,	ρ_x, ρ_y
Value:	0.01 m	0.01 m	69 GPa	0.3	2700 kg/m^3

Table 1: Geometrical and mechanical properties values of the beam grid.

Parameter:	l_x, l_y	d	E_p	ν_p	ρ_p
Value:	0.1 m	0.001 m	3 GPa	0.3	1200 kg/m^3

Table 2: Geometrical and mechanical properties values of the internal plates.

A structure of 20 by 20 cells is considered, with a total side length of $L = 2.21$ m. The extremities are clamped, and a point load is applied at the centre of the structure. The displacement fields are calculated by solving the analytical equation of the homogenised equivalent orthotropic plate model Eqn. (47) by finite element software. The fields are known on a grid of 91 by 91 regularly spaced points located on a window of side length $L_w = 1.808$ m centred on the entire domain. The frequencies range from 5 Hz to 500 Hz. The AKSI 2D method is applied to these fields and the extracted wavenumbers are compared with the analytical model. The results extracted by the AKSI 2D are shown in Figs. 10 and 11.

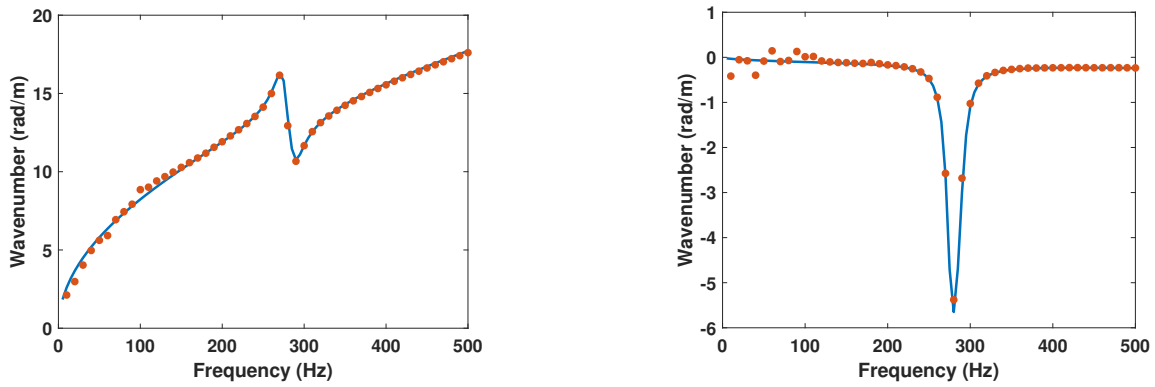

(a) (b)

Figure 10: Dispersion relation in the direction 0 rad of the bi-ribbed plate: (a) real part, (b) imaginary part. Analytical model (−) and wavenumber calculated with the AKSI 2D (•).

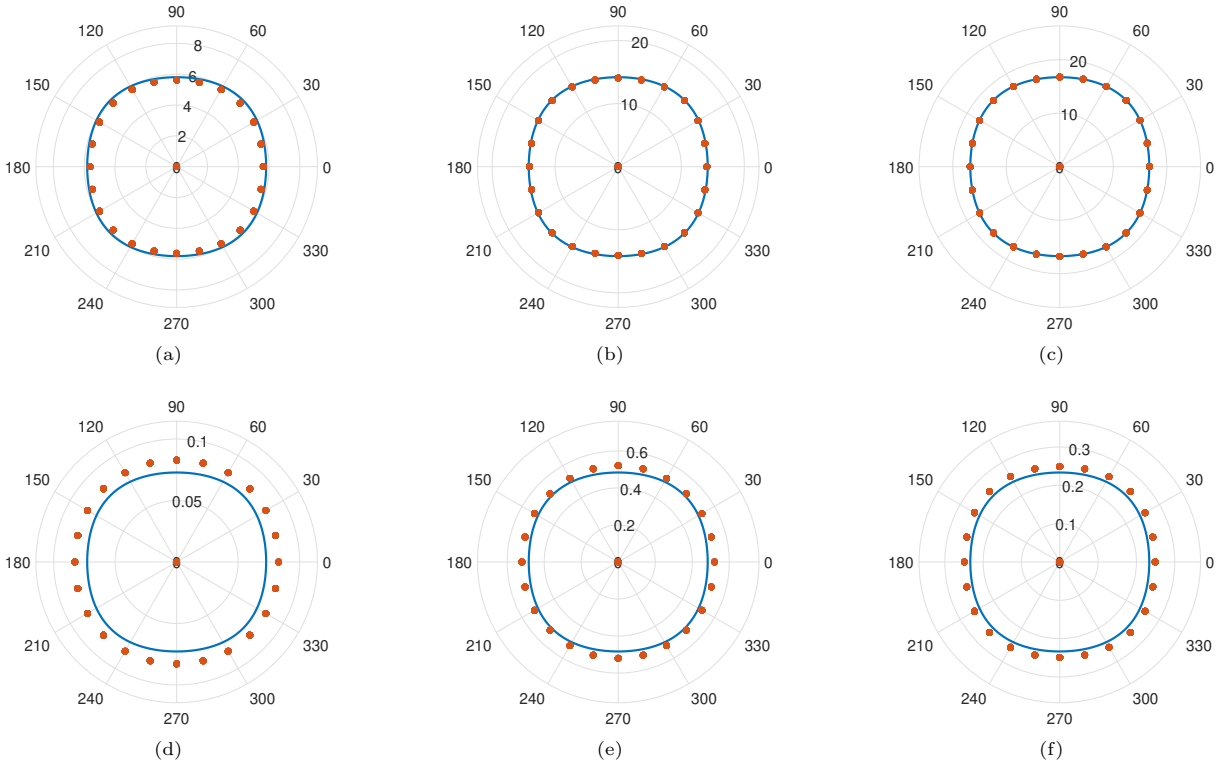

(a) (b) (c)

(d) (e) (f)

Figure 11: Real and imaginary parts of k-spaces of the bi-ribbed plate at three frequencies. Analytical model (−) and wavenumbers calculated with the AKSI 2D (•). (a) real part at 50 Hz, (b) real part at 250 Hz, (c) real part at 450 Hz, (d) imaginary part at 50 Hz, (e) imaginary part at 250 Hz and (f) imaginary part at 450 Hz.

Figs. 10 and 11 show that the wavenumbers are well calculated and match, those of the equivalent orthotropic plate model for most frequencies and directions. The inner resonance at 275 Hz is even very well retrieved for both the real and imaginary parts.

4. Experimental validation

This section is devoted to the experimental application of the AKSI 2D on a large-scale steel plate. The plate has dimensions of 0.95 m × 0.6 m, with a thickness of 2 mm. This steel plate has the same geometric properties as the analytical model of Section. 3. The experimental test is conducted by the Scanning Laser Doppler Vibrometer (SLDV). Fig. 12 shows the experimental setup where the plate was suspended at the fixed frame using Polylactic Acid filaments to approximate free-free boundary conditions. An electrodynamic shaker (Brüel & kJær, 4810) was used to generate a point mechanical force at the red point shown in Fig. 12. The shaker was attached to the structure using an impedance head and driven by a white noise signal over the frequency range from 0 Hz to 2500 Hz. A Polytec Scanning Vibrometer (PSV-400), placed approximately 1.2 m from the plate, was used to measure the full vibration field on a 48 × 55 mesh (sampling interval $\Delta x = 1.59$ cm and $\Delta y = 0.99$ cm). The scanning area of 0.747 m by 0.535 m is shown in the blue dotted rectangular box of Fig. 12. Finally, the displacement fields were acquired by a Fourier analyser installed in the measurement equipment. The vibrometer had the following setting parameters: the frequency resolution was 3.125 Hz, a Hanning window was applied to the time signals, a bandpass filter that includes the frequency range from 3.125 Hz to 2500 Hz was used, the overlap percentagewas 75% and 30 averages were taken by exponential averaging. The reference k-spaces are calculated with the usual mechanical parameter values of steel, so $E = 210$ GPa, $\nu = 0.3$, and $\rho = 7900\,\mathrm{kg/m^3}$.

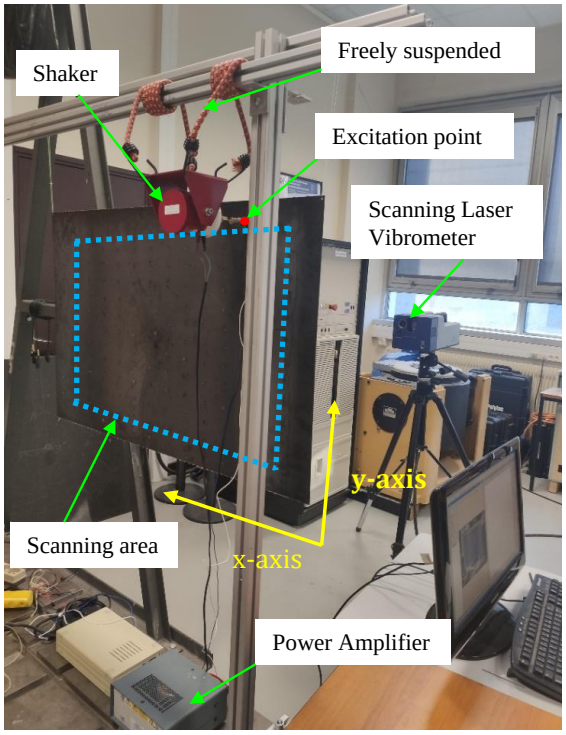

Figure 12: Experimental setup.

The comparison of complex wavenumber extracted by the AKSI 2D, the INCOME, and the IWC is shown in Fig. 13. From Fig. 13a which shows the extracted real part of the wavenumbers, it is clear to see that the AKSI 2D can provide a more accurate dispersion curve over the whole frequency range. However, it is worth noting that the imaginary parts of the wavenumbers extracted by these three methods are not acceptable for this experimental test. This is mainly because this plate with thin thickness has very low damping, resulting in the complexity of the displacement field influenced by multiple propagating waves and reflected waves. As a result, the local signal of the displacement field in this plate cannot be represented by a sum of exponential functions, which is contrary to the assumed model for these three methods. This leads

to the difficulty in extracting the imaginary part of wavenumbers. Finally, Fig. 14 compares the k-space extracted by the AKSI 2D, the IWC, and the INCOME, at two arbitrary frequencies, namely, 621 Hz and 1653 Hz. It can be seen that the AKSI 2D can provide more accurate results.

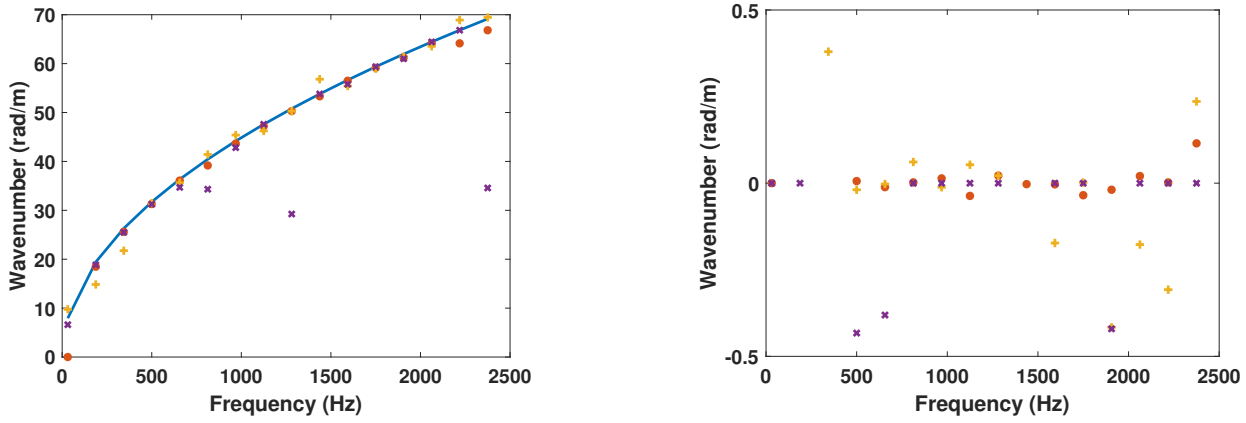

(a) (b)

Figure 13: Dispersion relation in the direction 0 rad of the experimental steel plate: (a) real part, (b) imaginary part. Analytical model (−) and wavenumber calculated with the AKSI 2D (•) the INCOME (+) and the IWC (x).

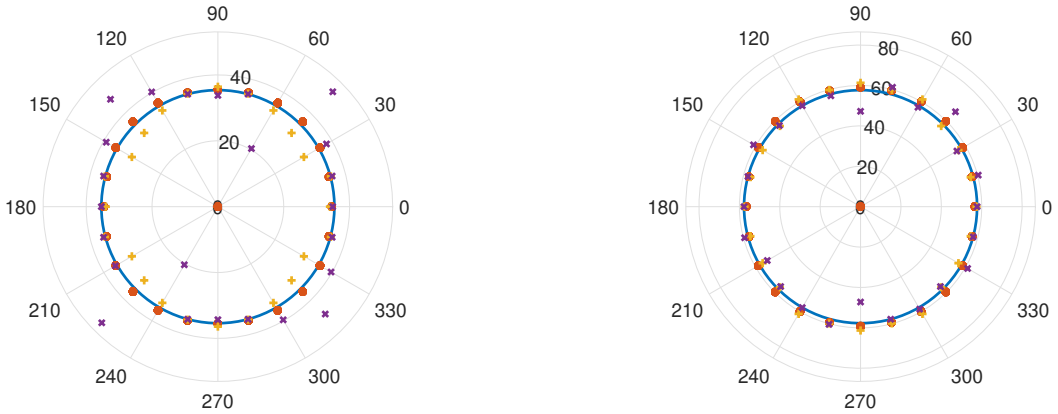

(a) (b)

Figure 14: Real parts of k-spaces of the experimental steel plate at 621 Hz (a) and 1653 Hz (b), extracted by analytical solution (−), the AKSI 2D (•), the INCOME (+) and, the IWC (x).

5. Conclusions

In this paper, a new inverse method, the Algebraic K-Space Identification 2D technique (AKSI 2D), is proposed for the extraction of the complex k-space elements from two-dimensional displacement fields. As compared to other popular 2D k-space techniques, like the IWC and the INCOME, the here-proposed method exhibits interesting performances in terms of efficiency and robustness when computing the complex k-spaces at relatively low frequencies. This is even more noticeable when handling noisy signals and position uncertainties.

In order to reach these conclusions, the formulations of the AKSI 2D are first presented thoroughly. Then, the proposed method is validated by by comparison with other inverse methods, including analytical, numerical, and experimental aspects. Therefore, for analytical validation purpose, the supporting test case

is a simply supported steel plate (Kirchhoff-Love plate). The results are derived from both exact and stochastic conditions. Among these uncertain conditions, a specific attention is addressed to signal noise and to position perturbations. The results are compared with those extracted by the IWC and the INCOME, which proves the ability of the method to extract complex k-spaces and damping loss factors under realistic conditions with better robustness than the other popular methods. The numerical validation is based on displacement fields that are extracted from the finite elements solution of a homogenised model. This study validates the effectiveness of the AKSI 2D for the complex k-space extraction for orthotropic structures. The experimental validation is performed on a steel plate with the same dimensions as those of the analytical case. This case illustrates that the AKSI 2D can extract complex k-spaces from real potentially noisy data.

This new method can provide interesting results for the k-space calculations in conditions beyond the operating area of previous methods. It overcomes some of their limitations and it appears to be efficient and robust for the calculation of complex k-spaces. However, the aftermath is that the AKSI 2D is more time-consuming compared to the INCOME when considering many measurements as input.

The proposed method has the potential to solve other vibroacoustic inverse problems, such as material characterisation, especially for the damping estimation using extracted complex k-spaces, and structural health monitoring.

CRediT authorship contribution statement

Thomas Brion: Conceptualization, Methodology, Software, Writing - original draft, Writing - review & editing. **Xuefeng Li**: Conceptualization, Methodology, Writing - original draft, Writing - review & editing. **Pascal Fossat**: Methodology, Writing - review & editing. **Mohamed Ichchou**: Conceptualization, Writing - review & editing, Validation, Project administration, Funding acquisition. **Olivier Bareille**: Writing - review & editing, Supervision, Project administration, Funding acquisition. **Abdel-Malek Zine**: Writing - review & editing, Supervision, Project administration, Funding acquisition.

Acknowledgments

This work was supported by the LabEx CeLyA (Centre Lyonnais d'Acoustique, ANR-10-LABX-0060) of Université de Lyon, within the program "Investissements d'Avenir" (ANR-11-IDEX-0007) operated by the French National Research Agency (ANR).

Appendix A. 2D k-space techniques

This appendix details the k-space methods for two-dimensional domains presented in the introduction and used as comparisons for the AKSI 2D in Section. 3.

Appendix A.1. Inhomogeneous Wave Correlation method

The Inhomogeneous Wave Correlation method, IWC, [12, 13] is an approach to calculate the k-space based on the maximisation of a correlation function between a displacement field $\hat{u}$ and an inhomogeneous wave $\hat{o}$. In two dimensions the inhomogeneous wave has the following definition, function of the direction, θ and the wavenumber given by k and γ, k being the real part of the wavenumber and γ the spatial decay, link with the imaginary part of the wavenumber.

$$\hat{o}_{k,\gamma,\theta}(x,y) = \mathrm{e}^{-\mathrm{i}k(\theta)(1+\mathrm{i}\gamma(\theta))(x\cos\theta+y\sin\theta)}. \tag{A.1}$$

For each direction, θ, the correlation function to maximise with k and γ is the following one.

$$IWC(k,\gamma,\theta) = \frac{\left|\iint_S \hat{u}.\hat{o}^*_{k,\gamma,\theta}\mathrm{d}x\ \mathrm{d}y\right|}{\sqrt{\iint_S |\hat{u}|^2\mathrm{d}x\ \mathrm{d}y.\iint_S |\hat{o}_{k,\gamma,\theta}|^2\mathrm{d}x\ \mathrm{d}y}}. \tag{A.2}$$

Numerical methods such as the trapezoidal method are used to calculate the integrals, since the field is only known at a discrete set of points. Moreover, the term $\iint_S \hat{u}^2 \mathrm{d}x\ \mathrm{d}y$ can be omitted as it is independent of θ, k and γ. The maximisation is done by evaluation. In the end, the method gives for each θ a value $k(\theta)$ and a value for $\gamma(\theta)$ and the complex wavenumber is $k(1+\mathrm{i}\gamma)$. By noting N the number of points in the discretisation and N_θ the number of directions. If the maximum search is done by evaluation, with $N_{\mathfrak{Re}}$ the number of values tested for the real part and $N_{\mathfrak{Im}}$ for the imaginary part, then the complexity of the IWC is around $\mathrm{O}(NN_\theta N_{\mathfrak{Re}} N_{\mathfrak{Im}})$.

Appendix A.2. INverse COnvolution MEthod

The INverse COnvolution MEthod (INCOME), [33] deals with another approach to calculate k-spaces. This method is inspired by the Prony method [29, 30, 31]. This method is more accurate and works at a lower frequency than the IWC method. However, it is not robust to noises or uncertainties, and it needs a regular grid of points. There are two steps in this method, first the calculation of a convolution kernel and then the deduction of the k-space. Let u be the discrete displacement field at a given frequency. The first step is to find a convolution kernel S such that:

$$u * S = 0, \tag{A.3}$$

or that at least minimise $\|u*S\|_2$. The form of S must be chosen a priori from the dimension of the problem, the complexity of the structure and the number of types of wave in the field. For example, the kernel Eqn. (A.4) can be used for an orthotropic field with one type of wave.

		f		
	d	c	d	
e	b	a	b	e
	d	c	d	
		f		

. (A.4)

For periodic structures, as explained in [34] for the case of the Prony method, the points put in relation together in the kernel have to be at the same position in the periodic cells. From the coefficient of S, the k-space will be deduced. The wavenumber in the θ direction is calculated by minimising of the module of a polynomial equation. For the example of an orthotropic plate, with a grid of spatial step $\Delta L_x\ \Delta L_y$ defining $\lambda_x(k,\theta) = \mathrm{e}^{\mathrm{i}k\cos\theta L_x}$ and $\lambda_y(k,\theta) = \mathrm{e}^{\mathrm{i}k\sin\theta L_y}$, the quantity to be minimised is the following:

$$\begin{aligned} I(\theta,k) = \Bigg| a + b\left(\lambda_x + \frac{1}{\lambda_x}\right) + c\left(\lambda_y + \frac{1}{\lambda_y}\right) + d\left(\lambda_x\lambda_y + \frac{1}{\lambda_x\lambda_y} + \frac{\lambda_y}{\lambda_x} + \frac{\lambda_x}{\lambda_y}\right) \\ + e\left(\lambda_x^2 + \frac{1}{\lambda_x^2}\right) + f\left(\lambda_y^2 + \frac{1}{\lambda_y^2}\right)\Bigg|. \end{aligned} \tag{A.5}$$

If N is the total number of points in the grid, then the complexity of the INCOME is of the order of $\mathrm{O}(N)$.

Appendix B. 2D Laplace transform

In the formulations Section. 2, the successive Laplace transforms are used:

$$\mathcal{L}_x\mathcal{L}_y\left[f(x,y)\right](s_x,s_y) = \int_0^{+\infty} \mathrm{e}^{-xs_x} \int_0^{+\infty} f(x,y)\mathrm{e}^{-ys_y}\mathrm{d}y\ \mathrm{d}x, \tag{B.1}$$

or

$$\mathcal{L}_y\mathcal{L}_x\left[f(x,y)\right](s_x,s_y) = \int_0^{+\infty} \mathrm{e}^{-ys_y} \int_0^{+\infty} f(x,y)\mathrm{e}^{-xs_x}\mathrm{d}x\ \mathrm{d}y. \tag{B.2}$$

In this appendix, some properties of the Laplace transform are presented. Let D be the derivative operator when the exponent is positive and the antiderivative operator when the exponent is negative.

$$\mathcal{L}\left[\mathrm{D}^{\alpha} f(t)\right](s) = s^{\alpha}\mathcal{L}\left[f(t)\right](s). \tag{B.3}$$

Here $-\alpha \in \mathbb{N}$.

$$\mathcal{L}\left[(-t)^{\beta} f(t)\right](s) = \frac{\mathrm{d}^{\beta}}{\mathrm{d}s^{\beta}}\mathcal{L}\left[f(t)\right](s), \tag{B.4}$$

for $\beta \in \mathbb{N}$. By combining the two previous properties, Eqn. (B.5) is deduced.

$$\mathcal{L}\left[\mathrm{D}^{\alpha}\left((-t)^{\beta} f(t)\right)\right](s) = s^{\alpha}\frac{\mathrm{d}^{\beta}}{\mathrm{d}s^{\beta}}\mathcal{L}\left[f(t)\right](s). \tag{B.5}$$

This property is used in Section. 2.

Appendix C. Numerical implementation

The implementation of the AKSI 2D method consists of three main steps.

- Calculation of the quantities $\phi_{ik}(x_0, y_0, x, y)$ using Eqn. (2).
- Deduction of the γ coefficients using Eqn. (1) by least squares resolution.
- Calculation of the k-spaces by polynomial resolution of Eqn. (3).

The first step is by far the most time-consuming but can be optimised a bit. For all the wanted pair of couples of point (x_0, y_0), (x, y) and for i and k from 0 to n_w, $\phi_{ik}(x_0, y_0, x, y)$ has to be calculated. Eqn. (1) is reminded just below.

$$\phi_{ik}(x_0, y_0, x, y) = \sum_{j=0}^{n_w}\sum_{l=0}^{n_w} \frac{(-1)^{j+l}(n_w+j)!(n_w+l)!\,(x-x_0)^{n_w-j}\,(y-y_0)^{n_w-l}}{j!(i+j)!(n_w-j)!l!(k+l)!(n_w-l)!} \times \int_{y_0}^{y}\int_{x_0}^{x}(y-y_1)^{k+l}(x-x_1)^{i+j}U(x_1,y_1)\mathrm{d}x_1\mathrm{d}y_1$$

If done directly, the calculation of all $\phi_{ik}(x_0, y_0, x, y)$ has a complexity of about $\mathrm{O}(n_w^6 N^3)$, where N the total number of points in the discretisation. However, some integrals are calculated more than once and some can be easily deduced from others. This appendix explains how the calculations have been done when the displacement field is known on a grid of $N = N_x \times N_y$ points. First, some intermediate quantities are defined:

$$J_n(x_0, x, y) = \int_{x_0}^{x}(x-x_1)^n U(x_1, y)\mathrm{d}x_1, \tag{C.1}$$

$$I_{nm}(x_0, x, y_0, y) = \int_{y_0}^{y}\int_{x_0}^{x}(y-y_1)^m(x-x_1)^n U(x_1,y_1)\mathrm{d}x_1\mathrm{d}y_1 = \int_{y_0}^{y}(y-y_1)^m J_n(x_0, x, y_1)\mathrm{d}y_1, \tag{C.2}$$

$$A_{ij} = \frac{(-1)^j(n_w+j)!}{j!(i+j)!(n_w-j)!}. \tag{C.3}$$

Therefore, $\phi_{ik}(x_0, y_0, x, y) = \sum_{j=0}^{n_w}\sum_{l=0}^{n_w} A_{ij}A_{kl}\,(x-x_0)^{n_w-j}\,(y-y_0)^{n_w-l}\,I_{i+j\,k+l}(x_0, x, y_0, y)$. The quantities are calculated step by step. First, all the quantities A_{ijkl} and integrals J_n needed are calculated, and then all the integrals I_{nm} are deduced. And finally the $\phi_{ik}(x_0, y_0, x, y)$ are calculated.

Appendix C.1. Calculations of J_n

First, all the integrations J_n are calculated. The approximation of the integrations uses the trapezoidal method. Let x_0 and x be abscissas of the grid of points such that $x_0 < x$. And Δx is the distance to the next abscissa of the grid. y is an ordinate of the grid and n goes from 0 to $2n_w$. The calculation of $J_n(x_0, x+\Delta x, y)$ can be reduced by using the knowledge of the $J_m(x_0, x, y)$ at the previous position (with $m \leq n$).

$$\begin{aligned} J_0(x_0, x+\Delta x, y) &= \int_{x_0}^{x} U(x_1, y)\mathrm{d}x_1 + \int_{x}^{x+\Delta x} U(x_1, y)\mathrm{d}x_1 \\ &\approx J_0(x_0, x, y) + \Delta x \frac{U(x, y) + U(x+\Delta x, y)}{2}, \end{aligned} \tag{C.4}$$

$$\begin{aligned} J_n(x_0, x+\Delta x, y) &= \int_{x_0}^{x} (x+\Delta x - x_1)^n U(x_1, y)\mathrm{d}x_1 + \int_{x}^{x+\Delta x} (x+\Delta x - x_1)^n U(x_1, y)\mathrm{d}x_1 \\ &\approx \sum_{l=0}^{n} \binom{n}{l} \Delta x^{n-l} J_l(x_0, x, y) + \Delta x^{n+1} \frac{U(x, y)}{2}. \end{aligned} \tag{C.5}$$

Using Eqn. (C.4) and (C.5), all integrations J_n are computed. In practice, the quantities are stored in a 3 dimension matrix. The first dimension is for all the pairs (x_0, x), the second for all the ordinates y and the third for all the values of n.

Appendix C.2. Calculations of I_{nm}

The next step is to deduce the quantities I_{nm} from the quantities J_n. Let y_0 and y be ordinates of the grid of points such that $y_0 < y$. And Δy is the distance to the next ordinate of the grid.

$$\begin{aligned} I_{n0}(x_0, x, y_0, y+\Delta y) &= \int_{y_0}^{y} J_n(x_0, x, y_1)\mathrm{d}y_1 + \int_{y}^{y+\Delta y} J_n(x_0, x, y_1)\mathrm{d}y_1 \\ &\approx I_{n0}(x_0, x, y_0, y) + \Delta y \frac{J_n(x_0, x, y) + J_n(x_0, x, y+\Delta y)}{2}, \end{aligned} \tag{C.6}$$

$$\begin{aligned} I_{nm}(x_0, x, y_0, y+\Delta y) &= \int_{y_0}^{y} (y+\Delta y - y_1)^m J_n(x_0, x, y_1)\mathrm{d}y_1 + \int_{y}^{y+\Delta y} (y+\Delta y - y_1)^m J_n(x_0, x, y_1)\mathrm{d}y_1 \\ &\approx \sum_{l=0}^{m} \binom{m}{l} \Delta y^{m-l} I_{nl}(x_0, x, y_0, y) + \Delta y^{m+1} \frac{J_n(x_0, x, y)}{2}. \end{aligned} \tag{C.7}$$

Using Eqn. (C.6) and (C.7), the quantities I_{nm} are calculated and stored. In practice, the quantities are stored in a 4 dimension matrix. The first dimension for all the couples of abscissa (x_0, x), the second for all the couples of ordinate (y_0, y), the third for all the values of n and the fourth for all the values of m.

Appendix C.3. Calculations of A_{ij}

The coefficients A_{il} are independent of the spatial coordinates, so they should be calculated once, stored in a matrix and then reused.

Appendix C.4. Calculation of ϕ_{ik}

Finally, the quantities $\phi_{ik}(x_0, y_0, x, y)$ are calculated using all the previous steps. With the proposed implementation, the complexity is approximately $\mathrm{O}(n_w^5 N^2)$.

$$\phi_{ik}(x_0, y_0, x, y) = \sum_{j=0}^{n_w} \sum_{l=0}^{n_w} A_{ijkl} \left(x - x_0\right)^{n_w - j} \left(y - y_0\right)^{n_w - l} I_{i+j\,k+l}(x_0, x, y_0, y). \tag{C.8}$$

References

[1] Z. Tian, W. Xiao, Z. Ma, L. Yu, Dispersion curve regression–assisted wideband local wavenumber analysis for characterizing three-dimensional (3d) profile of hidden corrosion damage, Mechanical Systems and Signal Processing 150 (2021) 107347.

[2] A. Santoni, S. Schoenwald, B. Van Damme, P. Fausti, Determination of the elastic and stiffness characteristics of cross-laminated timber plates from flexural wave velocity measurements, Journal of Sound and Vibration 400 (2017) 387–401.

[3] C. C. Claeys, K. Vergote, P. Sas, W. Desmet, On the potential of tuned resonators to obtain low-frequency vibrational stop bands in periodic panels, Journal of Sound and Vibration 332 (6) (2013) 1418–1436.

[4] G. Floquet, Sur les équations différentielles linéaires à coefficients périodiques, in: Annales scientifiques de l'École normale supérieure, Vol. 12, 1883, pp. 47–88.

[5] F. Bloch, Uber die quantenmechanik der elektronen in kristallgittern, z, Phys 52 (1928) 555.

[6] M. Collet, M. Ouisse, M. Ruzzene, M. Ichchou, Floquet–bloch decomposition for the computation of dispersion of two-dimensional periodic, damped mechanical systems, International Journal of Solids and Structures 48 (20) (2011) 2837–2848.

[7] J. B. J. Fourier, Théorie analytique de la chaleur, Vol. 1, Gauthier-Villars, 1888.

[8] P. Heckbert, Fourier transforms and the fast fourier transform (fft) algorithm, Computer Graphics 2 (1995) 15–463.

[9] S. Hambric, A. Barnard, Tutorial on wavenumber transforms of structural vibration fields, in: INTER-NOISE and NOISE-CON Congress and Conference Proceedings, Vol. 258, Institute of Noise Control Engineering, 2018, pp. 1–12.

[10] K. F. Chen, S. L. Mei, Composite interpolated fast fourier transform with the hanning window, IEEE Transactions on instrumentation and measurement 59 (6) (2010) 1571–1579.

[11] P. Podder, T. Z. Khan, M. H. Khan, M. M. Rahman, Comparative performance analysis of hamming, hanning and blackman window, International Journal of Computer Applications 96 (18) (2014) 1–7.

[12] J. Berthaut, M. Ichchou, L. Jezequel, K-space identification of apparent structural behaviour, Journal of Sound Vibration 280 (3-5) (2005) 1125–1131.

[13] M. Ichchou, O. Bareille, J. Berthaut, Identification of effective sandwich structural properties via an inverse wave approach, Engineering Structures 30 (10) (2008) 2591–2604.

[14] R. Cherif, J.-D. Chazot, N. Atalla, Damping loss factor estimation of two-dimensional orthotropic structures from a displacement field measurement, Journal of sound and vibration 356 (2015) 61–71.

[15] G. Tufano, F. Errico, O. Robin, C. Droz, M. Ichchou, B. Pluymers, W. Desmet, N. Atalla, K-space analysis of complex large-scale meta-structures using the inhomogeneous wave correlation method, Mechanical Systems and Signal Processing 135 (2020) 106407.

[16] M. Rak, M. Ichchou, J. Holnicki-Szulc, Identification of structural loss factor from spatially distributed measurements on beams with viscoelastic layer, Journal of Sound and Vibration 310 (4-5) (2008) 801–811.

[17] L. Van Belle, C. Claeys, E. Deckers, W. Desmet, On the impact of damping on the dispersion curves of a locally resonant metamaterial: Modelling and experimental validation, Journal of Sound and Vibration 409 (2017) 1–23.

[18] R. Lajili, O. Bareille, M. L. Bouazizi, M. Ichchou, N. Bouhaddi, Composite beam identification using a variant of the inhomogeneous wave correlation method in presence of uncertainties, Engineering Computations 35 (6) (2018) 2126–2164.

[19] R. Lajili, K. Chikhaoui, Z. Zergoune, M.-L. Bouazizi, M.-N. Ichchou, Impact of the vibration measurement points geometric coordinates uncertainties on two-dimensional k-space identification: Application to a sandwich plate with honeycomb core, Mechanical Systems and Signal Processing 167 (2022) 108509.

[20] G. Tufano, K-space analysis of complex large-scale periodic structures, Ph.D. thesis, Université de Lyon (France); Katholieke universiteit te Leuven (Belgium) (2020).

[21] R. Gunda, S. Vijayakar, R. Singh, Method of images for the harmonic response of beams and rectangular plates, Journal of Sound and vibration 185 (5) (1995) 791–808.

[22] M. N. B. Fazail, Damping loss factor characterization of complex structures using correlation method, Ph.D. thesis, Université de Technologie de Compiègne (France); Université de Sherbrooke, Québec (Canada) (2023).

[23] M. N. B. Fazail, J.-D. Chazot, G. Lefebvre, N. Atalla, Damping loss factor characterization of complex structures using a green's function-based model, Journal of Sound and Vibration 552 (2023) 117642.

[24] A. Geslain, S. Raetz, M. Hiraiwa, M. Abi Ghanem, S. Wallen, A. Khanolkar, N. Boechler, J. Laurent, C. Prada, A. Duclos, et al., Spatial laplace transform for complex wavenumber recovery and its application to the analysis of attenuation in acoustic systems, Journal of Applied Physics 120 (13).

[25] A. Cebrecos, V. Romero-García, J. P. Groby, Complex dispersion relation recovery from 2d periodic resonant systems of finite size, Applied Sciences 9 (3) (2019) 478.

[26] L. Schwan, A. Geslain, V. Romero-García, J.-P. Groby, Complex dispersion relation of surface acoustic waves at a lossy metasurface, Applied Physics Letters 110 (5).

[27] G. Yan, S. Raetz, J.-P. Groby, A. Duclos, A. Geslain, N. Chigarev, V. E. Gusev, V. Tournat, Estimation via laser ultrasonics of the ultrasonic attenuation in a polycrystalline aluminum thin plate using complex wavenumber recovery in the vicinity of a zero-group-velocity lamb mode, Applied Sciences 11 (15) (2021) 6924.

[28] G. R. de Prony, Essai experimental et analytique: sur les lois de la dilatabilite des fluides elastique et sur celles de la force expansive de la vapeur de l'eau et de la vapeur de l'alkool, a differentes temperatures, Journal Polytechnique ou Bulletin du Travail fait a l'Ecole Centrale des Travaux Publics.

[29] R. Kumaresan, D. W. Tufts, L. L. Scharf, A prony method for noisy data: Choosing the signal components and selecting the order in exponential signal models, Proceedings of the IEEE 72 (2) (1984) 230–233.

[30] J. J. Sacchini, W. M. Steedly, R. L. Moses, Two-dimensional prony modeling and parameter estimation, IEEE Transactions on signal processing 41 (11) (1993) 3127–3137.

[31] J. Casar-Corredera, J. Alcazar-Fernandez, L. Hernandez-Gomez, On 2-d prony methods, in: ICASSP'85. IEEE International Conference on Acoustics, Speech, and Signal Processing, Vol. 10, IEEE, 1985, pp. 796–799.
[32] P. Margerit, A. Lebée, J.-F. Caron, K. Ege, X. Boutillon, The high-resolution wavevector analysis for the characterization of the dynamic response of composite plates, Journal of Sound and Vibration 458 (2019) 177–196.
[33] R. F. Boukadia, C. Claeys, C. Droz, M. Ichchou, W. Desmet, E. Deckers, An inverse convolution method for wavenumber extraction (INCOME): Formulations and applications, Journal of Sound and Vibration 520 (2022) 116586.
[34] L. Ribeiro, V. Dal Poggetto, B. Huallpa, J. Arruda, Bloch wavenumber identification of periodic structures using prony's method, Mechanical Systems and Signal Processing 178 (2022) 109242.
[35] J. Cuenca, F. Gautier, L. Simon, Harmonic green's functions for flexural waves in semi-infinite plates with arbitrary boundary conditions and high-frequency approximation for convex polygonal plates, Journal of sound and vibration 331 (6) (2012) 1426–1440.
[36] N. Roozen, Q. Leclere, K. Ege, Y. Gerges, Estimation of plate material properties by means of a complex wavenumber fit using hankel's functions and the image source method, Journal of Sound and Vibration 390 (2017) 257–271.
[37] F. Ablitzer, C. Pézerat, B. Lascoup, J. Brocail, Identification of the flexural stiffness parameters of an orthotropic plate from the local dynamic equilibrium without a priori knowledge of the principal directions, Journal of Sound and Vibration 404 (2017) 31–46.
[38] F. Morandi, A. Santoni, P. Fausti, M. Garai, Determination of the dispersion relation in cross-laminated timber plates: Benchmarking of time-and frequency-domain methods, Applied Acoustics 185 (2022) 108400.
[39] X. Li, M. Ichchou, A. Zine, C. Droz, N. Bouhaddi, An algebraic wavenumber identification (awi) technique under stochastic conditions, Mechanical Systems and Signal Processing 188 (2023) 109983.
[40] M. Fliess, R. Marquez, Continuous-time linear predictive control and flatness: a module-theoretic setting with examples, International journal of control 73 (7) (2000) 606–623.
[41] M. Fliess, H. Sira-Ramirez, Closed-loop parametric identification for continuous-time linear systems via new algebraic techniques, Identification of Continuous-time Models from sampled Data (2008) 363–391.
[42] M. Fliess, H. Sira-Ramírez, An algebraic framework for linear identification, ESAIM: Control, Optimisation and Calculus of Variations 9 (2003) 151–168.
[43] E. Pereira, J. R. Trapero, I. M. Diaz, V. Feliu, Algebraic identification of the first two natural frequencies of flexible-beam-like structures, Mechanical Systems and Signal Processing 25 (7) (2011) 2324–2335.
[44] F. Beltrán-Carbajal, G. Silva-Navarro, Adaptive-like vibration control in mechanical systems with unknown paramenters and signals, Asian Journal of Control 15 (6) (2013) 1613–1626.
[45] X. Li, A. Zine, M. Ichchou, N. Bouhaddi, P. Fossat, An inverse method for characterization of dynamic response of 2d structures under stochastic conditions, Chinese Journal of Aeronautics.
[46] K. Schmüdgen, K. Schmüdgen, Discrete spectra of self-adjoint operators, Unbounded self-adjoint operators on Hilbert space (2012) 265–280.
[47] A. W. Leissa, Vibration of plates, Vol. 160, Scientific and Technical Information Division, National Aeronautics and Space Administration, 1969.
[48] R. H. Lyon, R. G. DeJong, M. Heckl, Theory and application of statistical energy analysis, second edition, The Journal of the Acoustical Society of America 98 (6) (1995) 3021–3021.
[49] F. Marchetti, K. Ege, Q. Leclère, N. B. Roozen, On the structural dynamics of laminated composite plates and sandwich structures; a new perspective on damping identification, Journal of Sound and Vibration 474 (2020) 115256.
[50] E. Manconi, B. R. Mace, Estimation of the loss factor of viscoelastic laminated panels from finite element analysis, Journal of Sound and Vibration 329 (19) (2010) 3928–3939.
[51] P. Margerit, A. Lebée, J.-F. Caron, X. Boutillon, High resolution wavenumber analysis (hrwa) for the mechanical characterisation of viscoelastic beams, Journal of Sound and Vibration 433 (2018) 198–211.
[52] C. Boutin, P. Fossat, C. Droz, M. Ichchou, Dynamics of ribbed plates with inner resonance: Analytical homogenized models and experimental validation, European Journal of Mechanics-A/Solids 79 (2020) 103838.
[53] W. C. Young, R. G. Budynas, A. M. Sadegh, Roark's formulas for stress and strain, McGraw-Hill Education, 2012.